INVESTIGATION OF THE MATERIAL PROPERTIES OF CERIUM OXIDE WITH DOPANTS FOR AN OXYGEN TRANSPORT MEMBRANE

by

James Morrow

B.S. Mechanical Engineering, Southern Illinois University, 2011

A Thesis
Submitted in Partial Fulfillment of the Requirements for the
Master of Science Degree in Mechanical Engineering.

Department of Mechanical Engineering and Energy Processes
in the College of Engineering
Southern Illinois University Carbondale
December 2017

www.manaraa.com

ProQuest Number: 10640175

All rights reserved

INFORMATION TO ALL USERS
The quality of this reproduction is dependent upon the quality of the copy submitted.

In the unlikely event that the author did not send a complete manuscript
and there are missing pages, these will be noted. Also, if material had to be removed,
a note will indicate the deletion.

ProQuest 10640175

Published by ProQuest LLC (2018). Copyright of the Dissertation is held by the Author.

All rights reserved.
This work is protected against unauthorized copying under Title 17, United States Code
Microform Edition © ProQuest LLC.

ProQuest LLC.
789 East Eisenhower Parkway
P.O. Box 1346
Ann Arbor, MI 48106 – 1346

www.manaraa.com

THESIS APPROVAL

INVESTIGATION OF THE MATERIAL PROPERTIES OF CERIUM OXIDE WITH DOPANTS FOR AN OXYGEN TRANSPORT MEMBRANE

By

James Morrow

A Thesis Submitted in Partial

Fulfillment of the Requirements

for the Degree of

Master of Science

in the field of Mechanical Engineering

Approved by:

Dr. Kanchan Mandal, Chair

Dr. Rasit Koc

Dr. James Mathias

Graduate School
Southern Illinois University Carbondale
November 3, 2017

www.manaraa.com

AN ABSTRACT OF THE THESIS OF

James Morrow, for the Master of Science degree in Mechanical Engineering, presented on November 3, 2017, at Southern Illinois University Carbondale.

TITLE: INVESTIGATION OF THE MATERIAL PROPERTIES OF CERIUM OXIDE WITH DOPANTS FOR AN OXYGEN TRANSPORT MEMBRANE

MAJOR PROFESSOR: Dr. Kanchan Mondal

Many physical properties of cerium oxide both undoped and doped have been studied herein. These properties include electrical conductivity, hardness, sintered density, and microstructure. These will be used to help determine a cerium oxide compound to use as an oxygen transport membrane in a combustion system. These compounds have been readily studied beforehand with exception to compounds with multiple dopants. Along with single doped cerium oxide, dual doped was investigated as well. The samples to be tested were created using co-precipitation and the subsequent powders were sintered at 1500°C to generate solid pellets. Once the pellets were formed the physical properties were tested. It was found that hardness and sintered density had little to no effect on electrical conductivity and the microstructures of the samples were shown to be favorable. As far as single or dual dopants were concerned, it was found that by including a second dopant along with zirconium that the electrical conductivity was reduced. Except for in the case where iron was doped along with zirconium, where the conductivity was increased. It was suggested to use samarium as the second dopant along with zirconium for the membrane.

www.manaraa.com

ACKNOWLEDGMENTS

I would like to thank Dr. Kanchan Mondal, my thesis advisor, who without out his guidance, support, and most of all patience, made the completion of this thesis possible. My gratitude is also extended to Dr. James Mathias and Dr. Rasit Koc, both for their assistance during the writing process which allowed the papers to be more clear and concise. Thanks also to Dr. Rasit Koc for allowing his laboratory and equipment to be used during the experimentation process of this research. Zhezhen Fu and Adam Sims, both for their help during the experimentation process, especially to Adam for his guidance during the entire process of this research. Lastly, I would like to thank my family and friends who never gave up on me even though it seemed that I had given up on myself.

www.manaraa.com

TABLE OF CONTENTS

www.manaraa.com

www.manaraa.com

LIST OF FIGURES

FIGURE PAGE

www.manaraa.com

www.manaraa.com

LIST OF TABLES

www.manaraa.com

LIST OF EQUATIONS

EQUATION PAGE

www.manaraa.com

CHAPTER 1

INTRODUCTION

1.1 Objective

The proposed research is expected to be used to determine the effect dopants have on cerium oxide's electrical conductivity and hardness. Many of the dopants proposed for this research have already been studied prior; however this research will also study the effects of doping cerium oxide with zirconium oxide plus another dopant. This information will then explicitly be used to choose the material combination which will make up an oxygen transport membrane for use in a combustion system. This research may also be used to further understand the effects of dopants on cerium oxide's ability to transport oxygen ions for use in solid oxide fuel cells and membranes for oxygen separation.

1.2 Literature Review

Ceramic oxygen transport membranes have been studied greatly over the last 40 years. Not only can these membranes be used in fuel cells, but can also be used in processes where high oxygen purity is needed. These membranes can also be worked into a catalytic membrane reactor allowing oxidation and catalysis to occur simultaneously. For example, petrochemistry processes and ammonia oxidation during nitric acid manufacturing can use this technique [1].

Two types of oxygen transport membranes exist: pure ionic, and mixed ionic and electronic. Both types require a potential difference to allow the transport of oxygen ions. The pure ionic type requires an external circuit to allow the flow of electrons from one side to the other to maintain a charge balance within the membrane. Alternatively,

www.manaraa.com

the mixed ionic and electronic type can allow electron flow within the membrane itself, so that only a difference in oxygen partial pressure across the membrane is required to allow oxygen ion flow. These mixed ionic and electronic membranes are generally an ionic type ceramic doped with an electronic type ceramic [1].

The most common structure types for these ceramic membranes are fluorite and perovskite. The fluorite structure is a simple cubic packing of the anions with half of the cation sites being occupied. Doping a metal oxide compound with a fluorite structure with a metal oxide with a lower valence will tend to have a higher electrical conductivity due to higher oxygen mobility. This happens because many of the oxygen anion sites go unfilled which leads to an oxygen deficiency. Perovskites have a more complex structure than fluorites. Two common perovskites are $CaTiO_3$ and $SrTiO_3$ which have a cubic structure with an octahedral formation off each side of the cube. For example, in $SrTiO_3$, Ti is at the corners of the cube, Sr is at the center, and oxygen atoms are on the centers of the edges forming a TiO_6 octahedral. Generally, perovskites have higher ionic and electronic conductivity than fluorites. However, the focus of this research was on fluorites, specifically doped cerium oxide [1].

It is known that the ionic and electronic properties of the ceramic oxygen transport membranes are due to defects within the compound. A higher defect quantity will tend to raise the entropy of the structure. As the temperature increases, the defect amount will increase also increasing the entropy. This increase defect quantity will tend to increase both the ionic and electronic properties of the structure. These defects come in two types, electronic and structural [1].

www.manaraa.com

There are many preparation methods for ceramic compounds. These include conventional power methods, co-precipitation, sol-gel, alkoxide-salt route, citrate complexation route, hydrothermal, and spray and freeze drying. Each method can result in differing microstructures that impact conductivity. These differences are things such as porosity and grain size [1].

Cerium oxide has been an area of focus as it is a great alternative material to be used in solid oxide fuel cells (SOFCs). By using cerium oxide the working temperature of the SOFC can be lowered as cerium oxide has increased ionic conductivity at lower temperatures near 1000K. This lower working temperature will have many positive effects on SOFCs, including longer lifespan and allowing the use of different materials elsewhere in the SOFC [2-6].

A United States patent details an oxygen ion transport membrane. This membrane is of a composite nature consisting of a non-porous layer which allows only oxygen ions flow through as well as electron movement to balance the charge effect of the ions. This layer is comprised of two sublayers. The first sublayer is scandium oxide doped, yttrium or cerium stabilized zirconia, while the second is a metal oxide consisting of lanthanum, strontium, chromium, manganese, vanadium, and cerium. While cerium may be present in these layers, it is never present in high percentages [7]. This shows that much research has gone into the study of oxygen transport membrane technology, but not the use of cerium oxide as the largest constituent, although it has been shown to have high ionic and electronic conductivities.

Much research has been focused on doped cerium oxide. Most of this research focuses on using trivalent and divalent anions as dopants. This is due to cerium being

www.manaraa.com

of 4+ valences and having a fluorite structure when oxidized. When cerium oxide is doped with a metal of lower valence, oxygen vacancies will occur readily. These vacancies should increase the materials overall ionic and electronic conductivity. This change in conductivity may be related to the atomic radius of the dopants and the ability for the overall fluorite structure to remain intact [6].

The characterization of metal oxides has taken place using the same equipment previously used by both Rayford and Kong [8-9]. Each of these researchers characterized the electrical conductivity of cermets using titanium carbide and tungsten carbide. The measurement was performed through the use of a sample holder allowing a resistance to be measured using a four-wire setup. The sample holder was used to allow for use within a furnace, so the temperature could be increased to the range of interest. The methodology and apparatus used by Rayford and Kong is very similar for the proposed research [8-9].

www.manaraa.com

CHAPTER 2

METHOD

2.1 Creating Powders

There is a desire to arrive at powders that consist of only cerium oxide and oxides of the desired dopants. It has been decided to synthesize these powders through co-precipitation. Each of the metals is obtainable in a few forms. It has been devised to purchase each of the metals to be used as a nitrate compound. These nitrates are very stable and will dissolve readily into deionized water. This will aid in the chemical reaction required to obtain the oxide compounds desired. The amounts of the nitrates used, were such that, on a molar basis 5% of the total was the metal dopant with the remaining portion being that of cerium. Mixing the nitrates, hexamethylenetetramine (HMTA), and sodium dodecyl sulfate in deionized water will take place initially. Gradually adding heat to the mixture begins to break down the HMTA releasing ammonia which will produce ammonium ions by reacting with hydrogen ions in the water. This will then allow the metallic ions to react with the hydroxide ions leftover in the water, thus producing metal hydroxides. Heat was added until the mixture reaches 95C and allowed to remain for one hour. The mixture was cooled at room temperature. The precipitates were then filtered out using a Buchner funnel and an ashless paper filter. These precipitates were then heated to 105°C and 650°C, remaining at each 1 hour and 6 hours, respectively. The remaining water was boiled off at 105°C and the calcination process took place at 650°C. Following this heating process the powders that remained were the metal oxides desired. Figure 1 shows an image of one of the doped powders containing cerium, yttrium, and zirconium oxides.

www.manaraa.com

Fig.1: $Ce_{0.9}Y_{0.05}Zr_{0.05}O_2$ Powder

2.2 Creating Pellets

2.2.1 Pressureless Sintering

As the doped cerium oxide is desired as a solid pellet, additional steps need to be taken. The powders synthesized previously were mixed with binding agent, polyvinyl alcohol (PVA). This will allow the powders to bind together better during the pressing process. Next this mixture was pressed together inside of a round steel form at 4 metric tons which over the 6.35 mm diameter of the press is 1279 MPa. This uniaxial pressure was held for 10 minutes. This press formed pellet was placed into a vacuum oven at 70°C to allow the alcohol from the binder to evaporate. Finally, the pressed pellet was placed into a tube furnace to allow sintering. This sintering will occur at 1500°C or 1300°C if iron is present, for 6 hours. Figure 2 shows the form that the powder is placed into to be pressed. Figure 3 shows the final sintered pellet after being cut into smaller samples for further testing.

www.manaraa.com

Fig. 2: Pellet Form

Fig. 3: Cut Pellet

2.2.2 Pressured Sintering

This method was similar to the above method. However, the pressing and sintering will occur simultaneously and no binding agent needs to be used. The pressure and temperatures used were the same as before. The form was made of graphite so that it can withstand the higher temperatures while carrying the press load. This process will occur under vacuum as to not ignite the graphite form. It is expected that this method will result in higher densities. Figure 4 shows the hot pressing unit that was used. The manufacturer is Materials Research Furnaces, Inc.

www.manaraa.com

Front Loading Physical Test Vacuum Furnace
Model No.: HP-12x12-G-G-(W-W/M)-2400-VG

Fig. 4: Hot Press

www.manaraa.com

2.3 Sintered Density Measurement

The sintered density of each pellet was measured by means of Archimedes principle. The dry weight was measured followed by the weight of the pellet while it was suspended in water. The difference in the weight is the buoyancy force of the water acting upwards on the pellet. This force is the weight of the water displaced. As the density of the water can be determined from the temperature of the water, the mass of water displaced is related to the volume of the water displaced. With the volume of the water displaced being equal to the volume of the pellet. Now with the mass and volume of the pellet known, the sintered density was calculated.

The sintered density of each pellet was compared to the theoretical density of each compound. From these two values, the relative density was calculated. The theoretical density was determined from the results of the energy-dispersive X-ray spectroscopy (EDS) measurement, which gives precise amounts of the present elements. It is expected that the relative density will affect all other properties of each pellet.

2.4 Electrical Conductivity

For cerium oxide to allow oxygen ions to move through its structure, a charge balance, in the form of electrons flowing through the structure, needs to occur. The ultimate desire is to have ability to flow electrons faster than oxygen ions, so that oxygen flow is not impeded. Therefore, the electrical conductivity was measured through a desired temperature range. This process will utilize a resistance bridge to measure the resistance across the specimen. The resistance bridge uses the four-wire

www.manaraa.com

method for measuring resistance allowing the resistance in the wires and other parts of the system to be ignored. First, each sample pellet to be tested was cut to form a rectangular piece which was tested. The specimen is placed inside an alumina holder so that it can be placed inside a furnace and the closed circuit will remain intact. The temperature of the furnace was then increased from room temperature up to 1100°C. Resistance values were recorded every 100°C once a resistance within the range of the bridge could be measured.

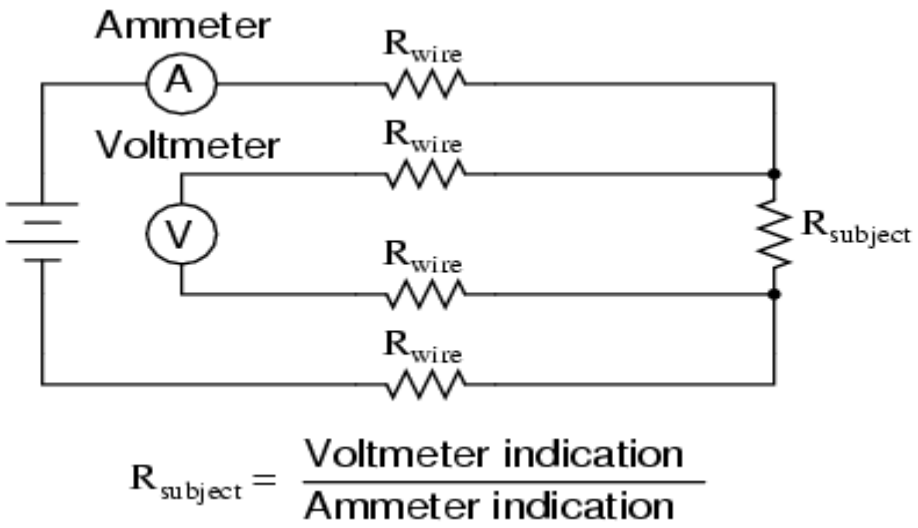

Fig. 5: Four Wire Method

With the resistance and dimensions of the specimen known, the conductivity can then be calculated. While conductivity can be compared directly between specimens for given temperatures or range of temperatures, it also may be helpful to compare using an exponential equation for electron conduction:

$$\sigma = \frac{\sigma_0}{T} exp\left(-\frac{E_a}{k_B T}\right) \quad (1)$$

Where σ is electrical conductivity, σ_0 is a temperature independent pre-exponential factor, T is the absolute temperature, E_a is the activation energy for conductivity, and k

www.manaraa.com

is the Boltzmann constant. Equation 1 shows that when 1/T versus ln(σT) is plotted, the result is a straight line with a slope of $-E_a/k$ and an intercept of σ_0. From this slope, the activation energy was calculated.

2.5 Hardness

The hardness of each compound was measured. The hardness is needed as the end material chose will need to fit tightly in a system where the temperature will change. This means if the membrane material expands more than the system surrounding it that there will be stress put upon the membrane, so the hardness of the material needs to be such that it will not crack while undergoing theses stresses.

To measure the hardness, a Vickers hardness tester was used. This tester utilizes an automatic indenter and a computer to calculate the hardness based on the size of the indentation.

2.6 Differential Scanning Calorimetry

Differential scanning calorimetry (DSC) was used to calculate the specimen's specific heat capacity through a range of temperatures. The DSC does this by comparing the amount of heat required to raise the temperature of the sample to that of a standard. As this standard has a well-documented specific heat capacity over the desired temperature range, this comparison will allow the calculation of the specimen's specific heat capacity. With the specific heat capacity known, the amount of energy required to raise and maintain the membrane material to working temperature can be determined.

www.manaraa.com

2.7 Imaging/Chemical Makeup

X-ray diffraction (XRD) and scanning electron microscopy in conjunction with energy dispersive x-ray spectroscopy was used to provide different types of imaging. XRD allowed the structure of the solids to be known. With the structure known, it is possible to estimate how electrons and ions will flow through the structure. It is expected that all compounds tested will have the same Fluorite cubic structure as standard cerium oxide. Figure 6 shows an example of the XRD testing for the cerium oxide specimen. The image shows the data compared to the standard data for that of cerium oxide.

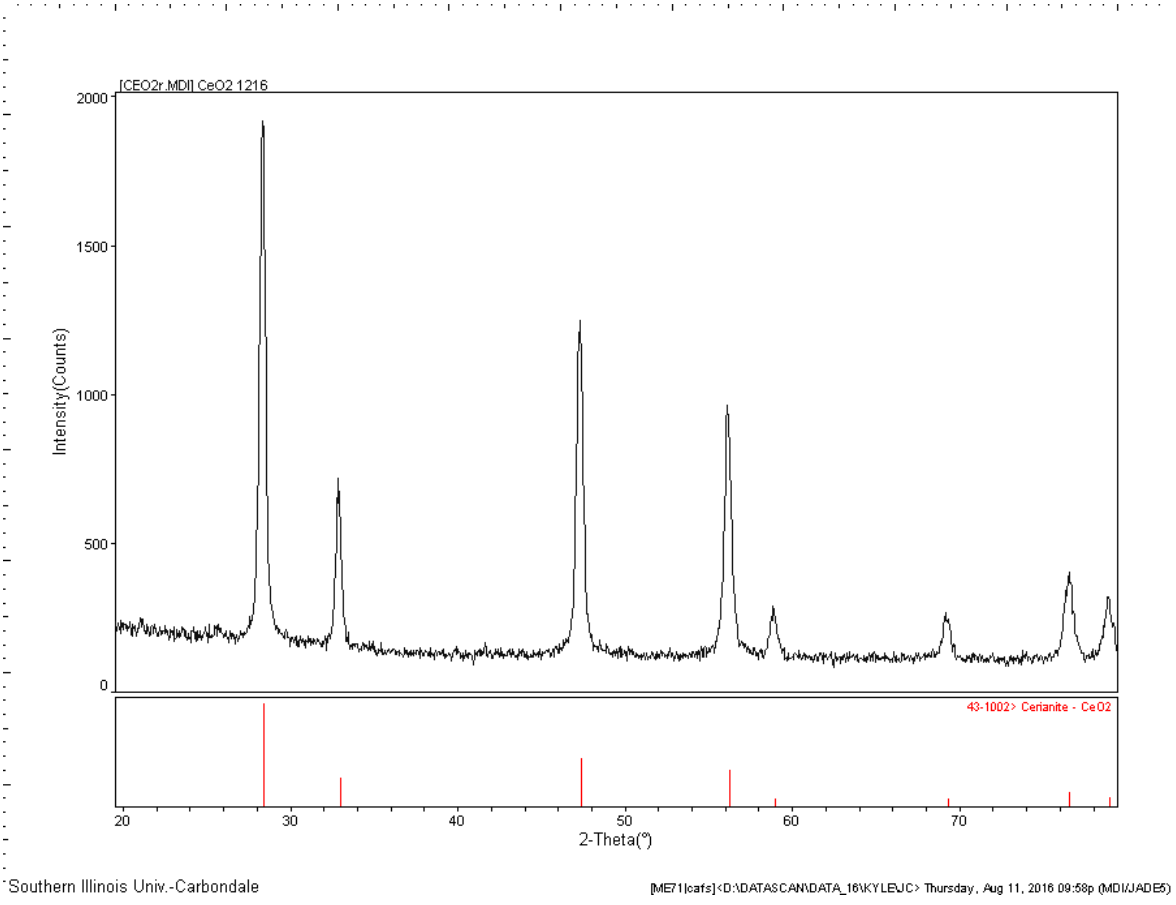

Fig. 6: XRD for Cerium Oxide

www.manaraa.com

Scanning Electron Microscopy (SEM) provided surface imaging of the pellets and powders being tested. For the pellets, the average grain size was calculated, thereby giving additional information about the sintered density and hardness of each sample. As for the imaging of the powders, this will gave an understanding of how the grains were created from the powders used in the sintering process. Figure 7 shows an SEM image of yttria and zirconia doped ceria. This image was used to determine the average grain size of the sample and gave an idea of its porosity.

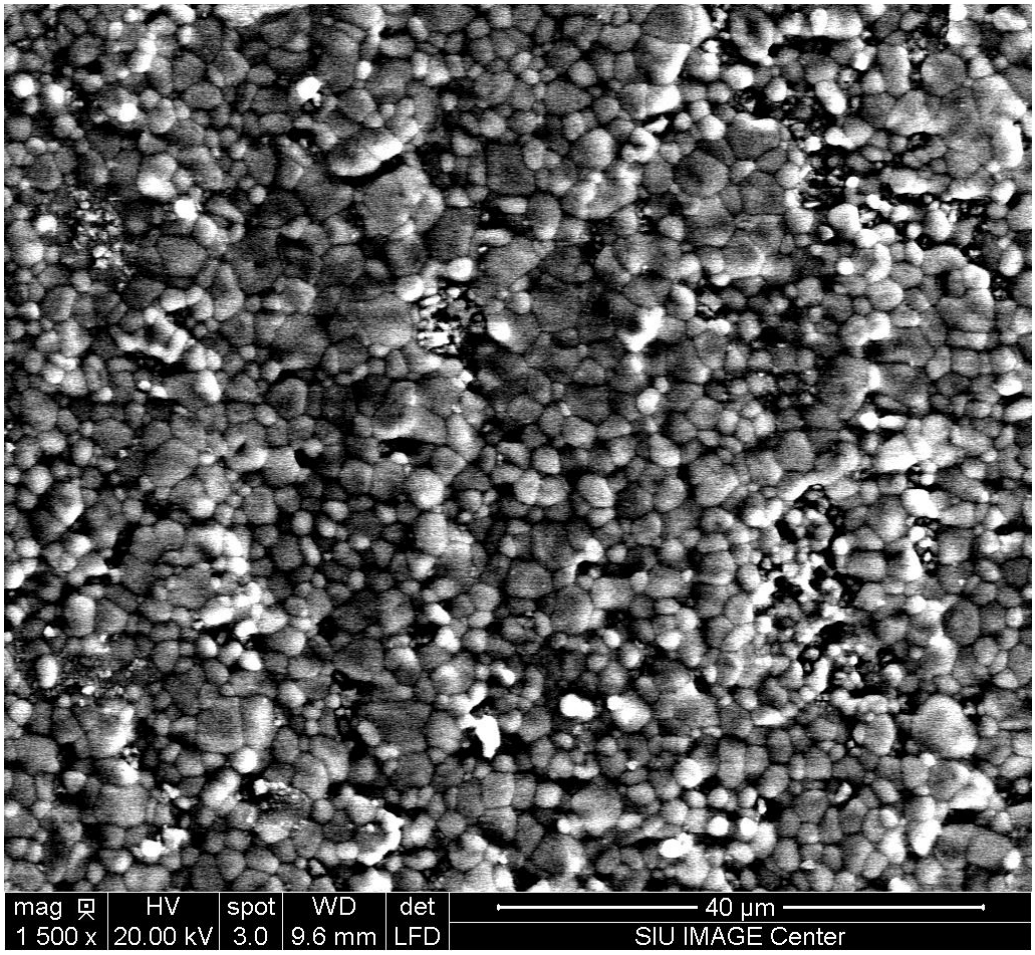

Fig. 7: SEM Image of Yttria and Zirconia doped Ceria

Energy-dispersive X-ray spectroscopy (EDS) provided a better understanding of the exact elemental makeup of the specimens. This allowed the theoretical density of the pellets to be calculated. EDS was also used to provide a surface scan showing the

www.manaraa.com

dispersion of individual elements throughout the pellets surface. This scan provided information about whether there is a large grouping of the dopants in only a few locations or whether the dopants are evening spread throughout the pellet.

www.manaraa.com

CHAPTER 3

RESULTS

Figures, 8 and 9, show the natural log of the product of conductivity and temperature versus the inverse of temperature. Plotting the electrical conductivity this way is useful because σ_0 and E/k from equation 1 are the y-intercept and slope, respectively, of the trends for each material. Figures, 10 and 11, show sintered density and hardness for each sample.

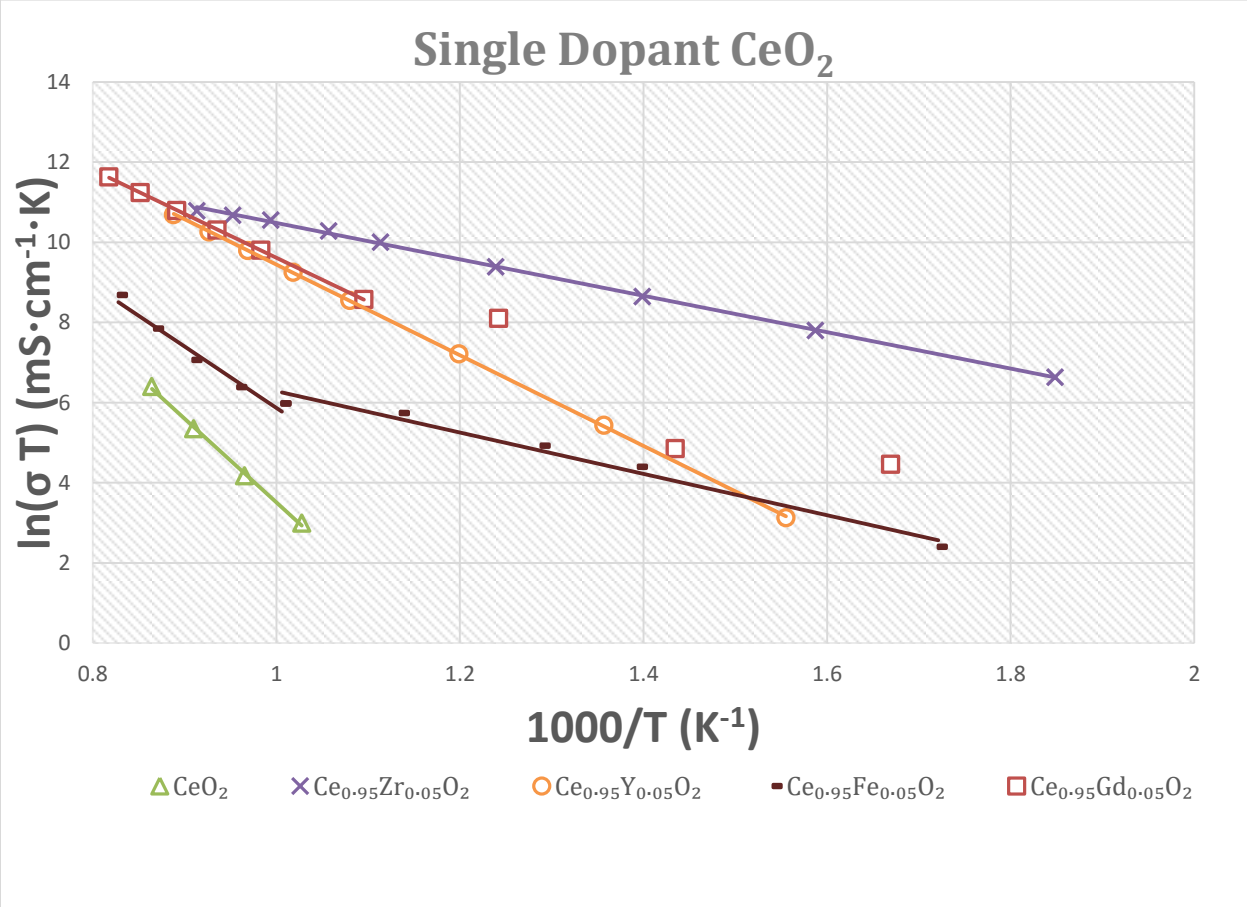

Fig. 8: Conductivity of Single Doped Cerium Oxide

www.manaraa.com

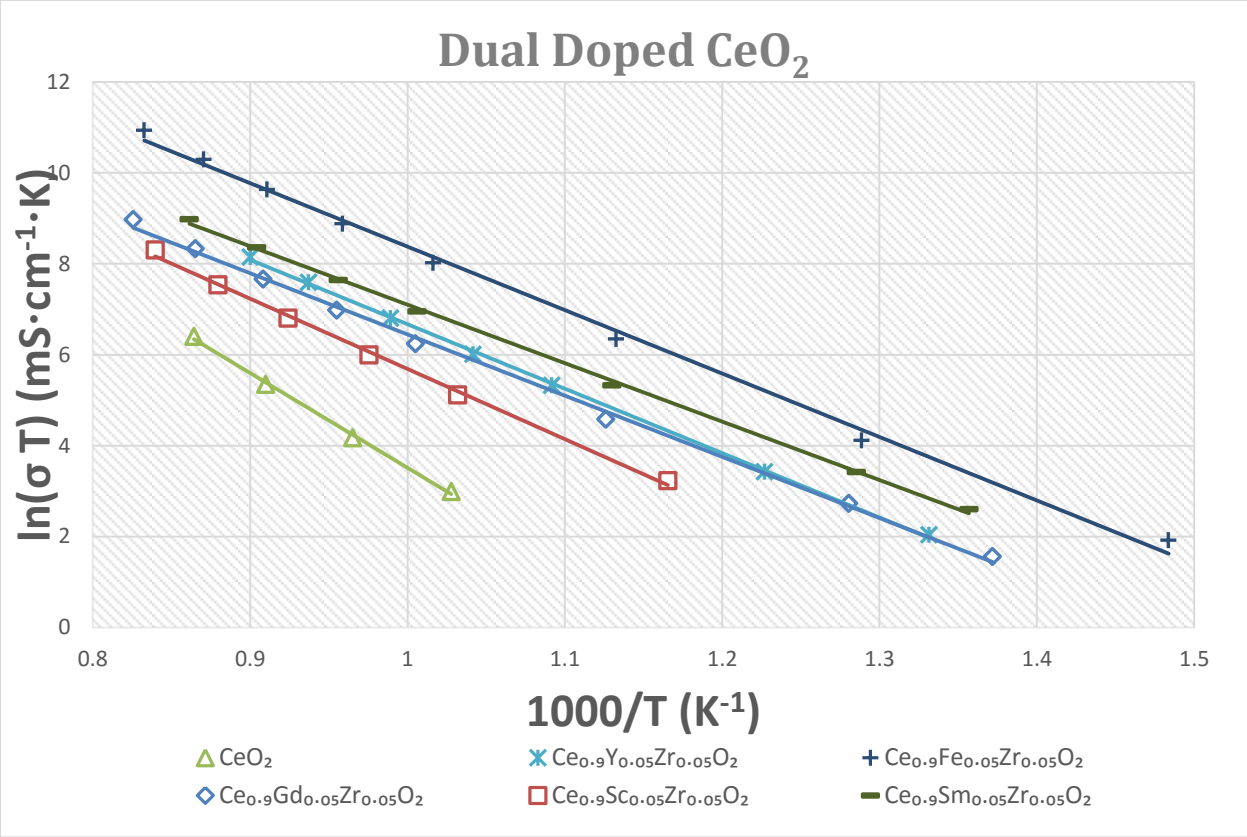

Fig. 9: Conductivity of Double Doped Cerium Oxide

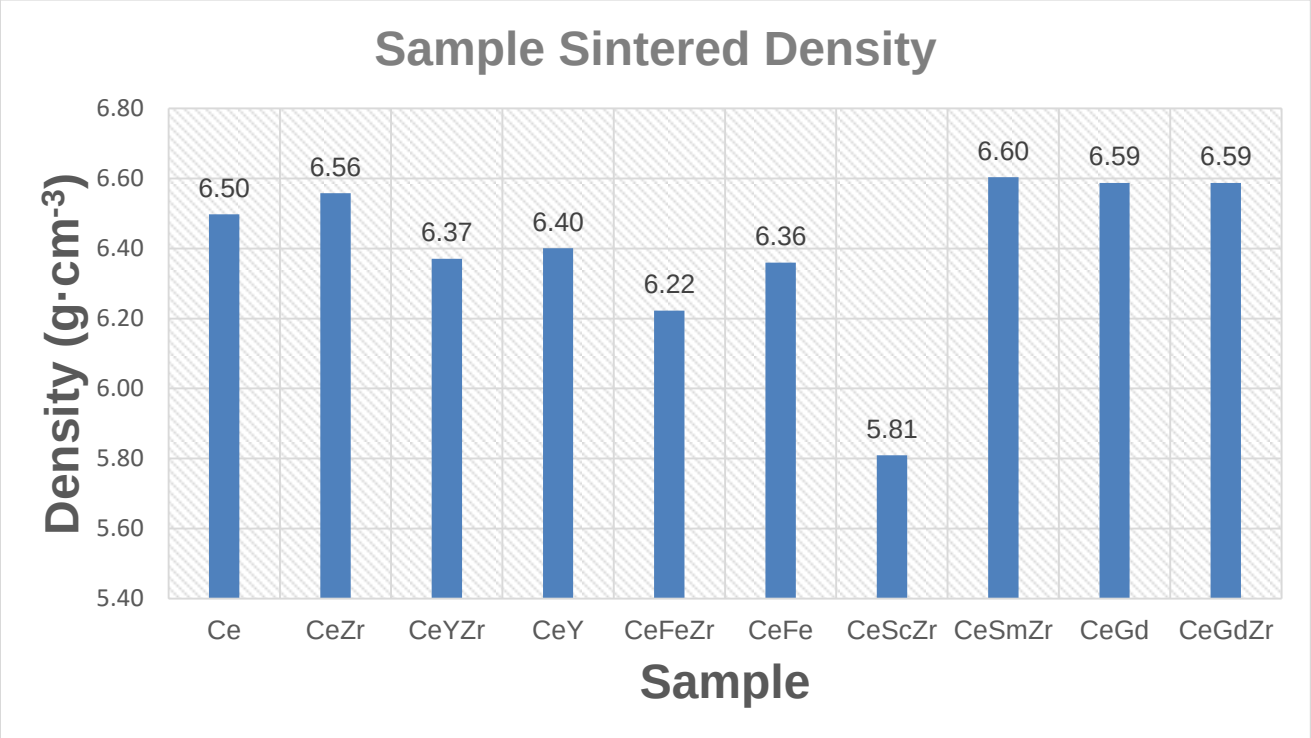

Fig. 10: Sample Sintered Density

www.manaraa.com

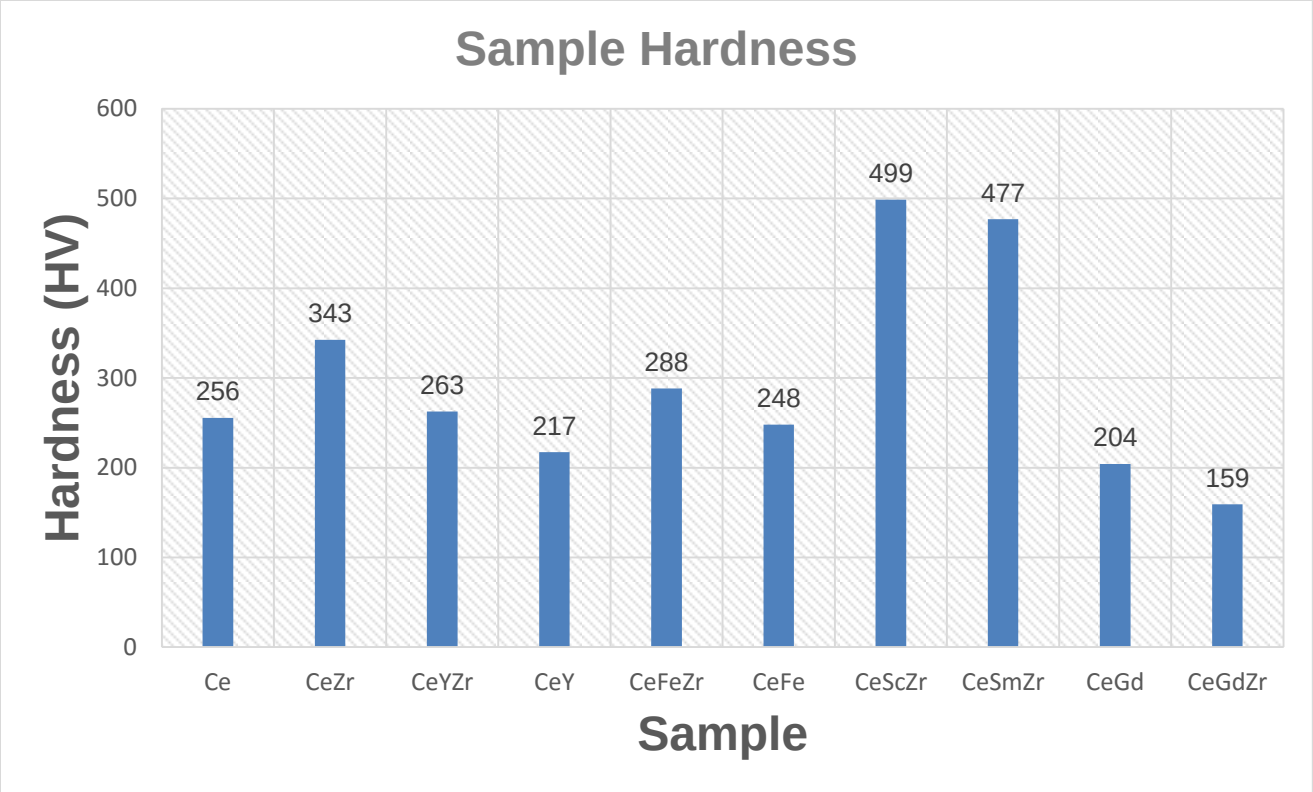

Fig. 11: Sample Hardness

Figures 12 through 21 show the XRD for all specimens. These are used to show the overall structure of each sample. These samples all show to have the same structure with very little differences as the undoped cerium oxide structure. This means that the dopants will have taken the place of the cerium in the overall structure, but may have displaced some of the oxygen, resulting in holes that may allow oxygen ions to flow through the structure.

www.manaraa.com

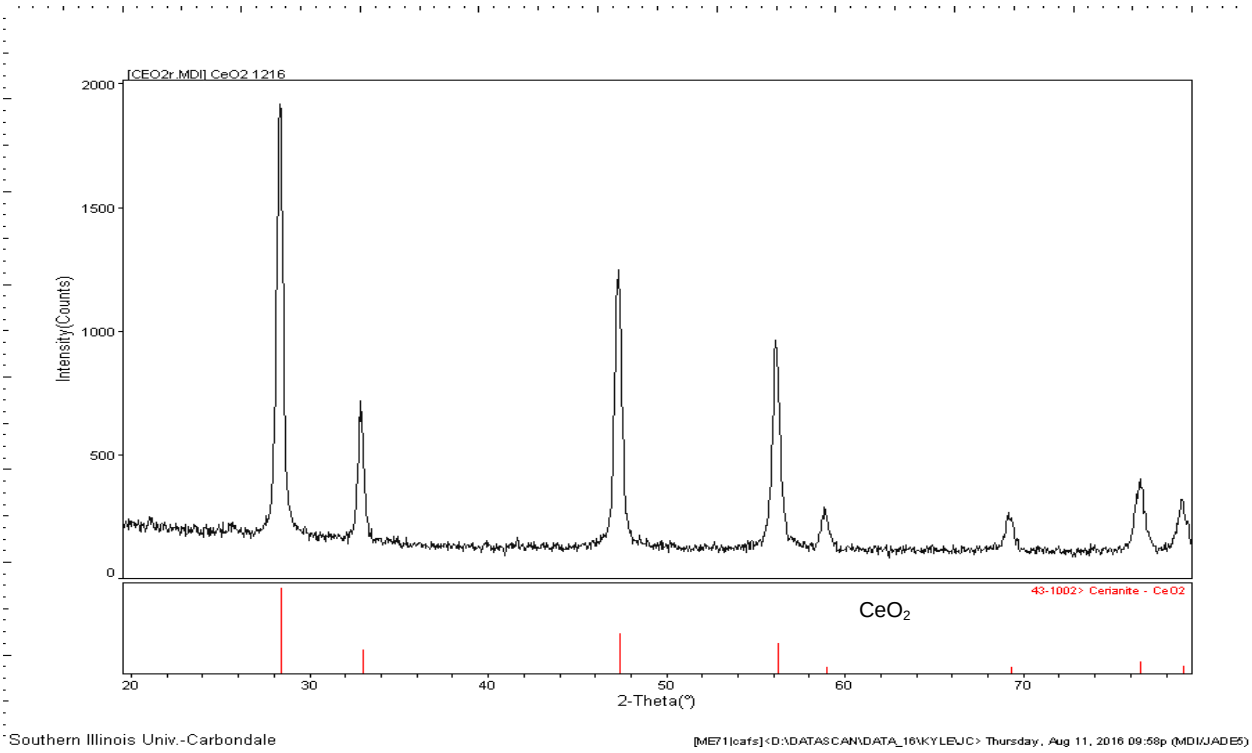

Fig. 12: XRD of CeO_2

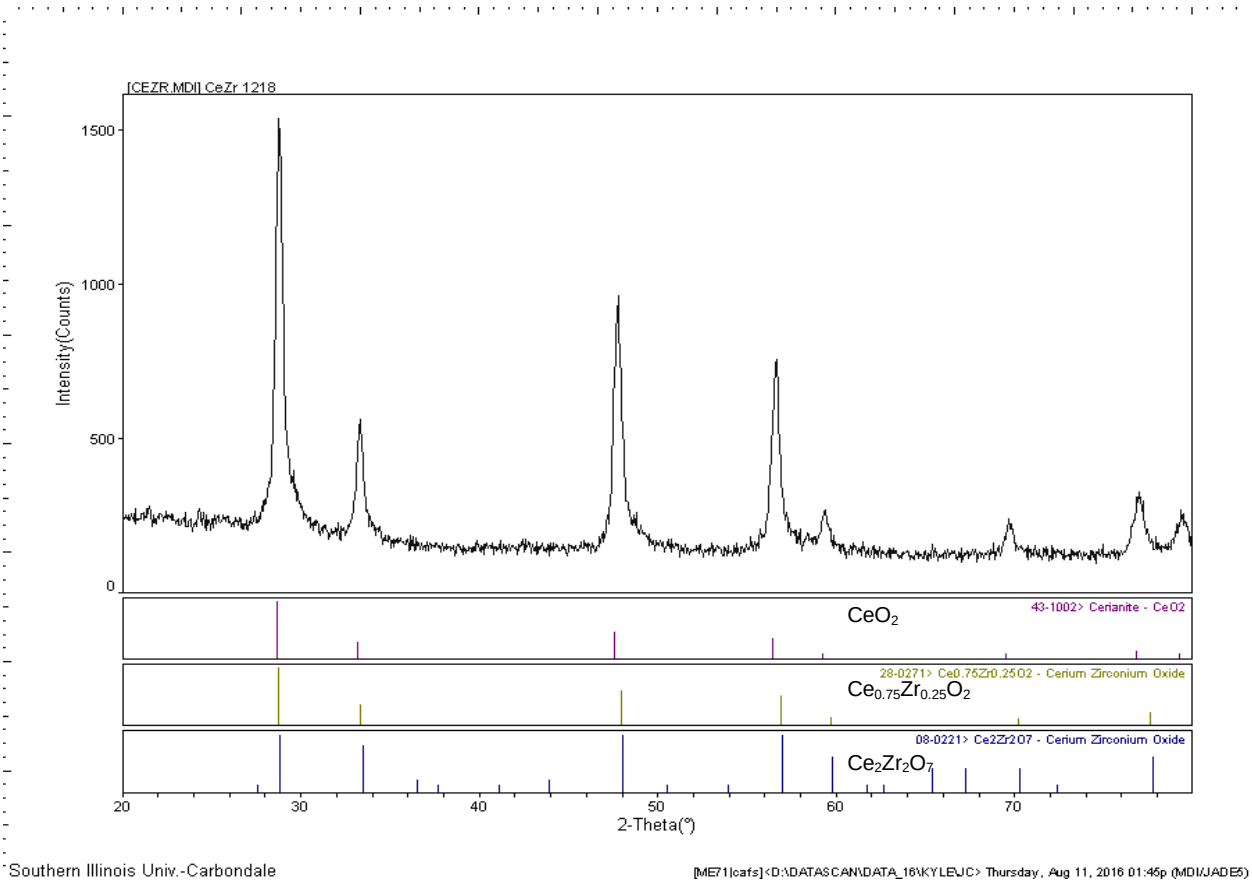

Fig. 13: XRD of $Ce_{0.95}Zr_{0.05}O_2$

www.manaraa.com

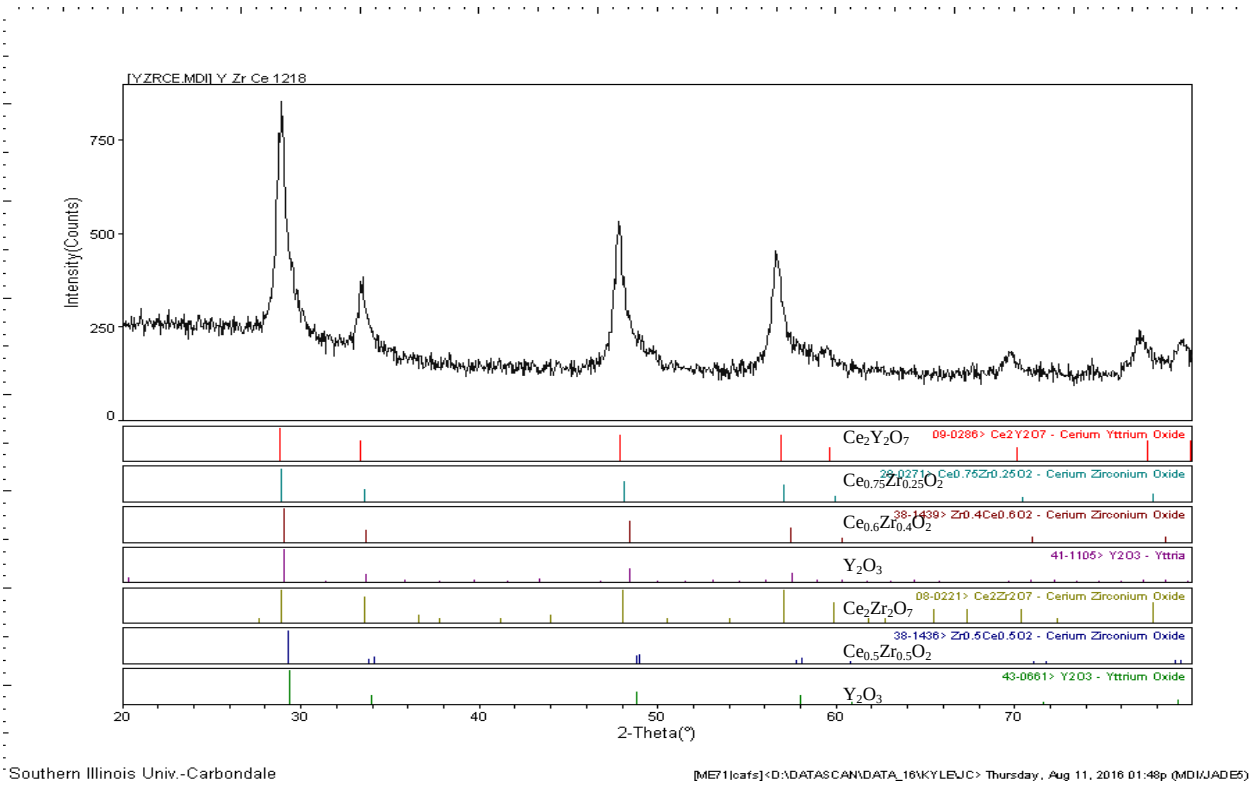

Fig. 14: XRD of $Ce_{0.9}Y_{0.05}Zr_{0.05}O_2$

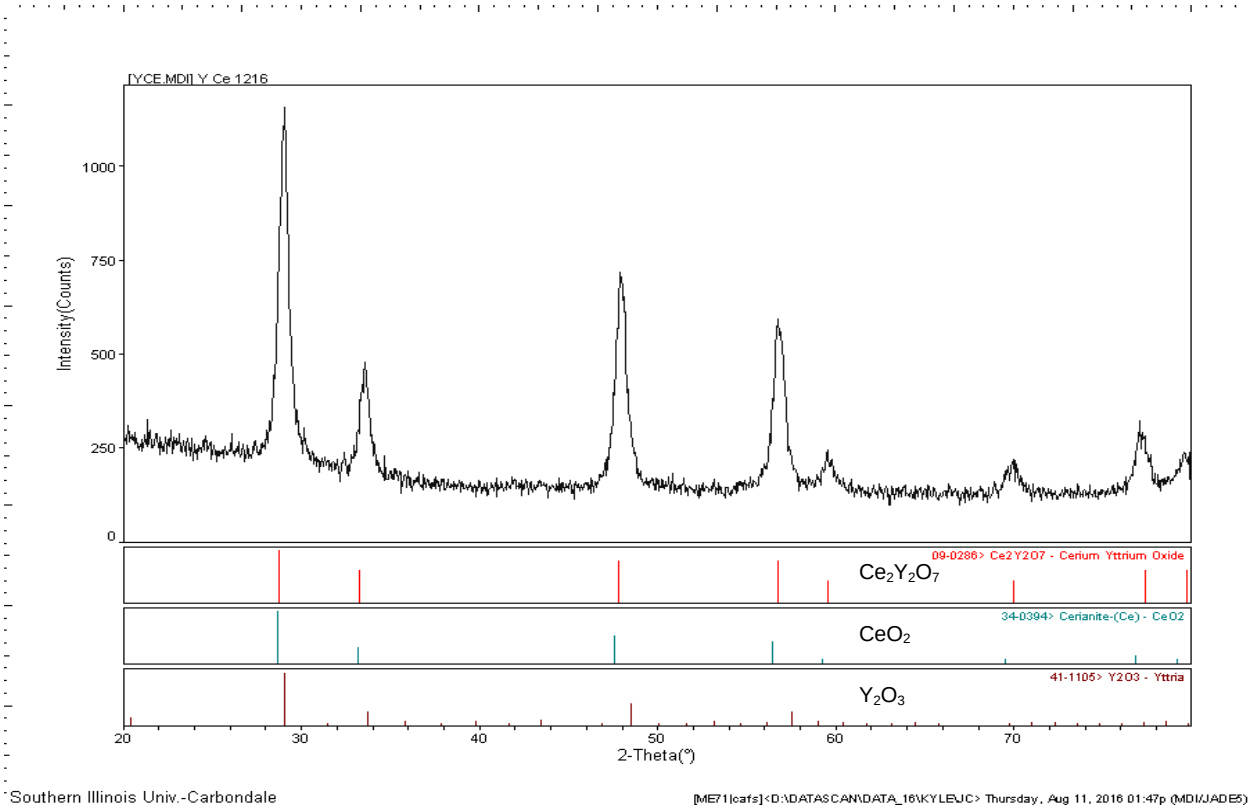

Fig. 15: XRD of $Ce_{0.95}Y_{0.05}O_2$

www.manaraa.com

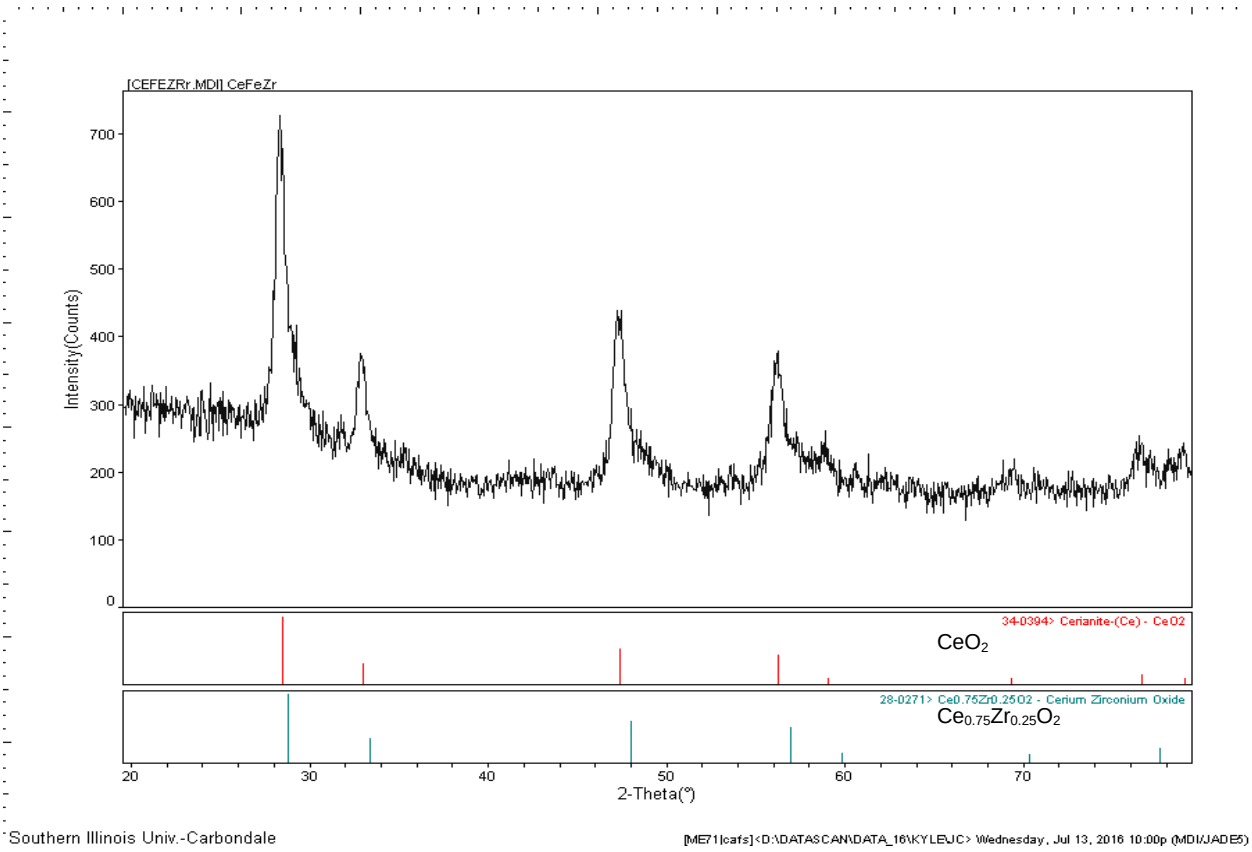

Fig. 16: XRD of CeFeZr

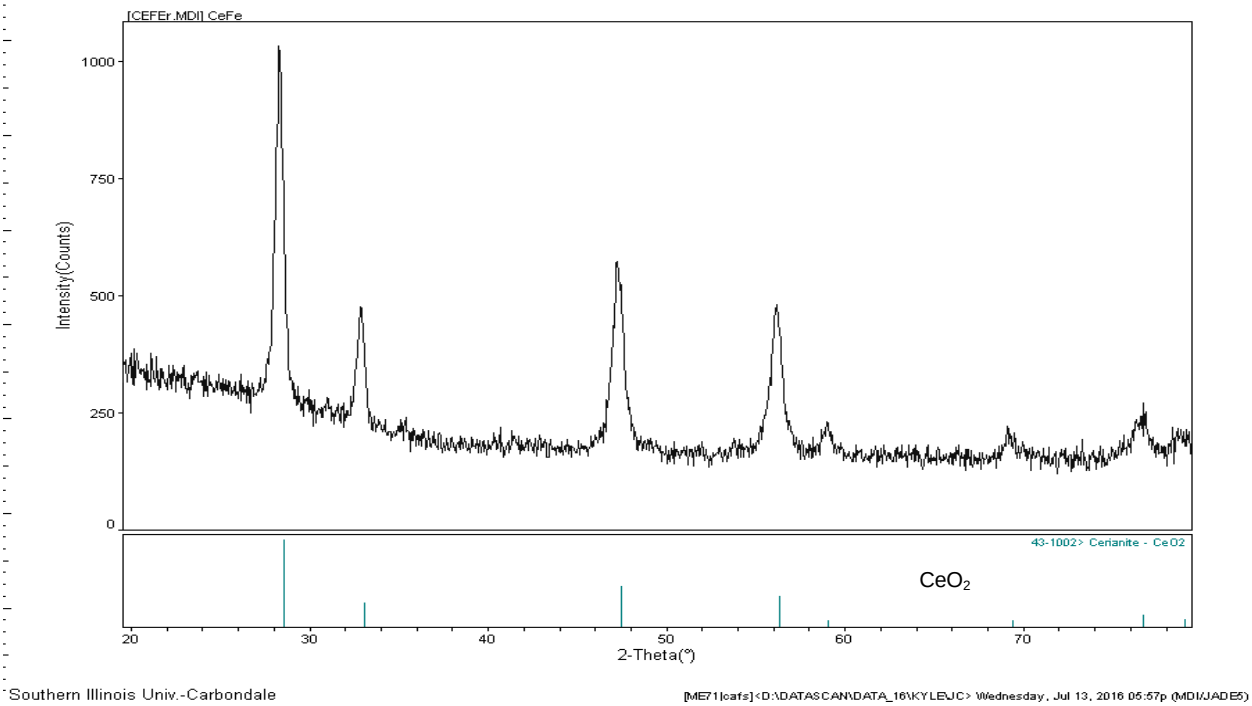

Fig. 17: XRD of $Ce_{0.95}Fe_{0.05}O_2$

www.manaraa.com

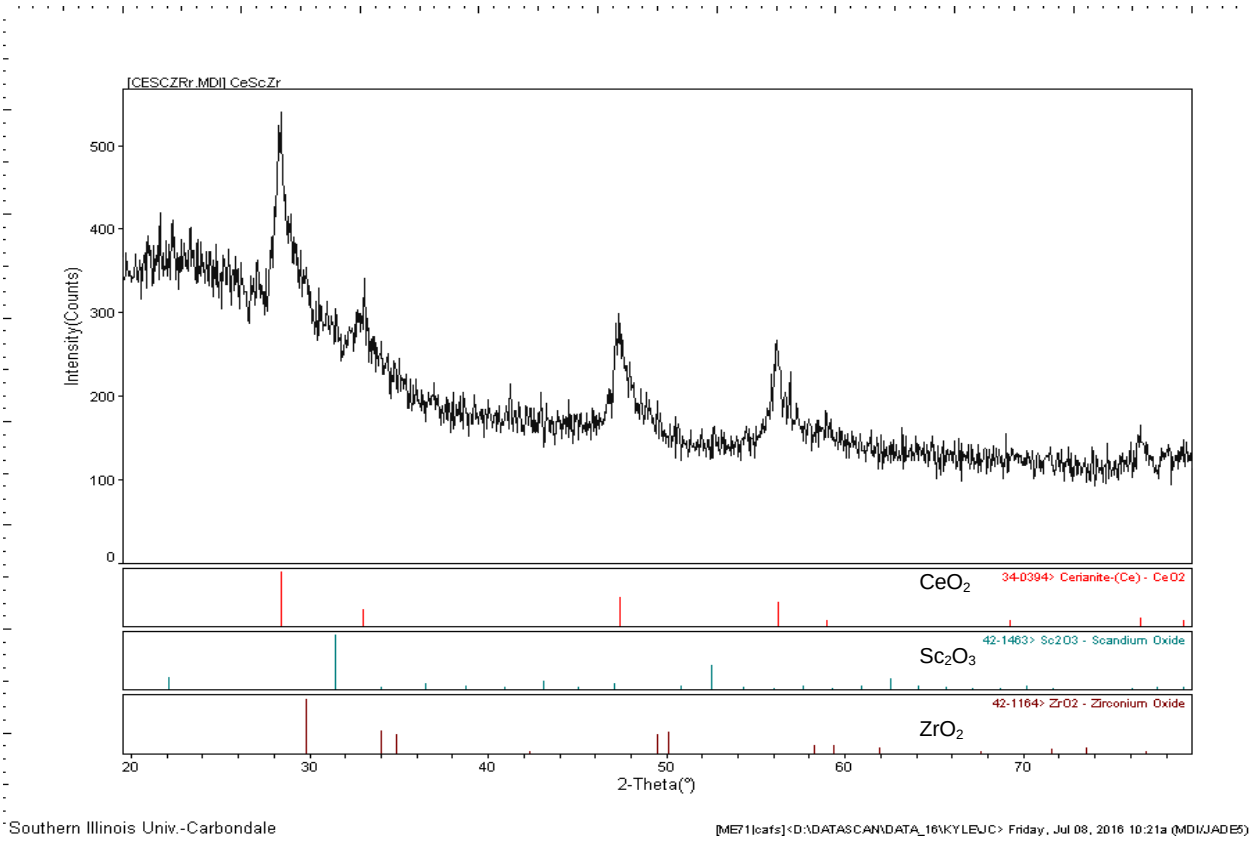

Fig. 18: XRD of $Ce_{0.9}Sc_{0.05}Zr_{0.05}O_2$

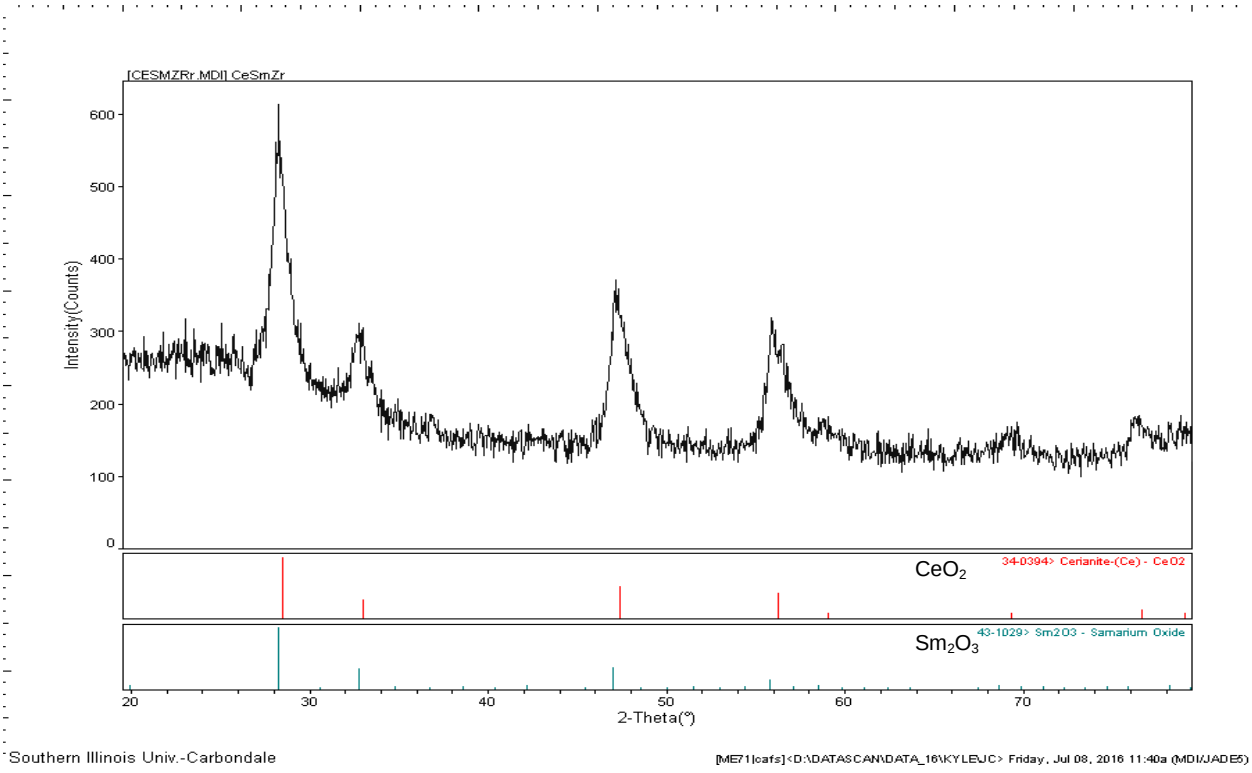

Fig. 19: XRD of $Ce_{0.9}Sm_{0.05}Zr_{0.05}$

www.manaraa.com

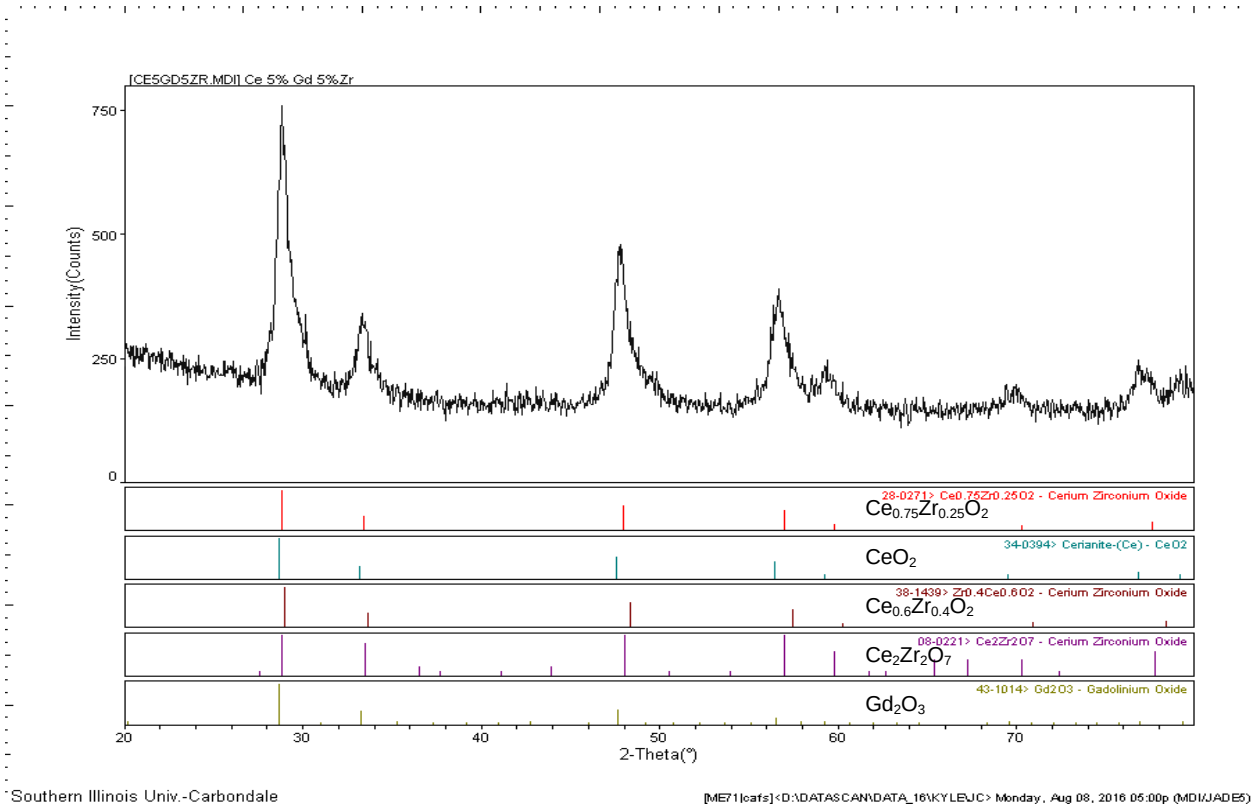

Fig. 20: XRD of $Ce_{0.9}Gd_{0.05}Zr_{0.05}O_2$

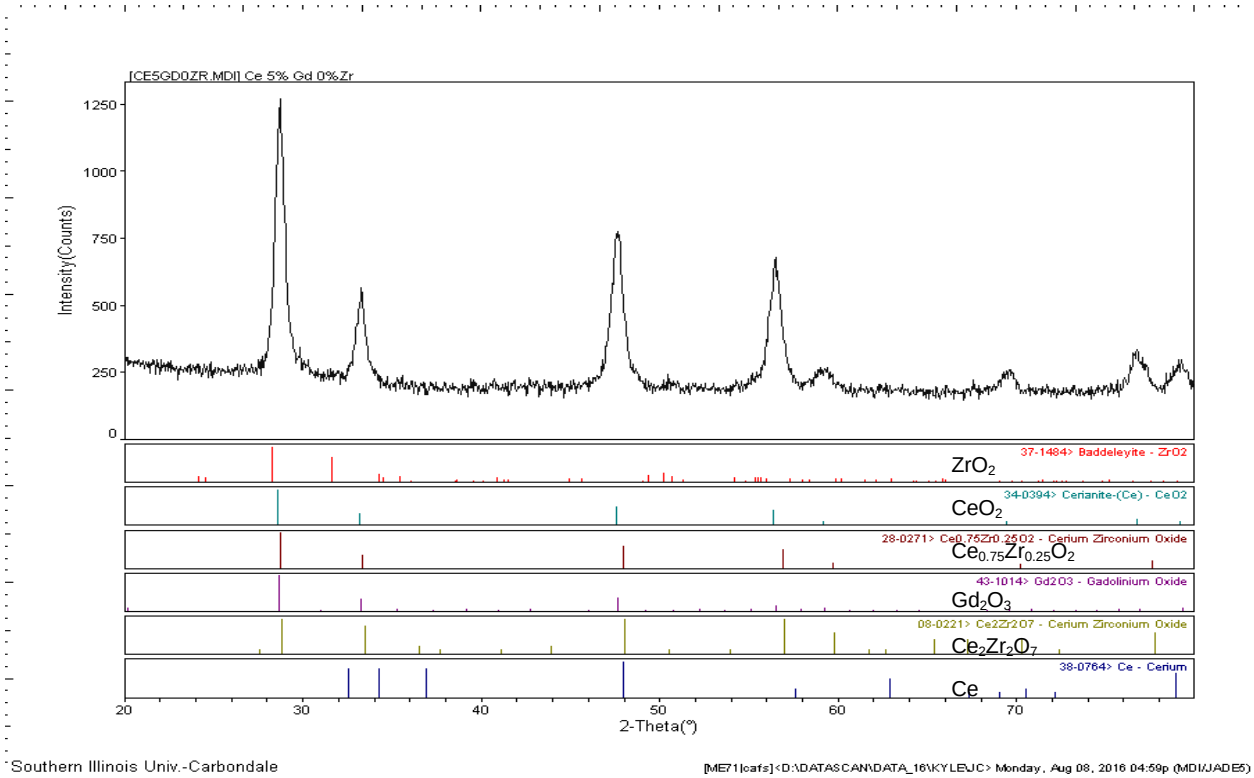

Fig. 21: XRD of $Ce_{0.95}Gd_{0.05}O_2$

www.manaraa.com

Figures 22 through 26 show the surface imaging of CeO_2, $Ce_{0.9}Y_{0.05}Zr_{0.05}O_2$, $Ce_{0.95}Zr_{0.05}O_2$, $Ce_{0.9}Sc_{0.05}Zr_{0.05}O_2$, and $Ce_{0.9}Sm_{0.05}Zr_{0.05}O_2$ that were completed using SEM. These images allow the knowledge of grain size uniformity and porosity over the portion of the surface that was imaged to be obtained. This also allows the average grain size of each specimen to be compared to the others.

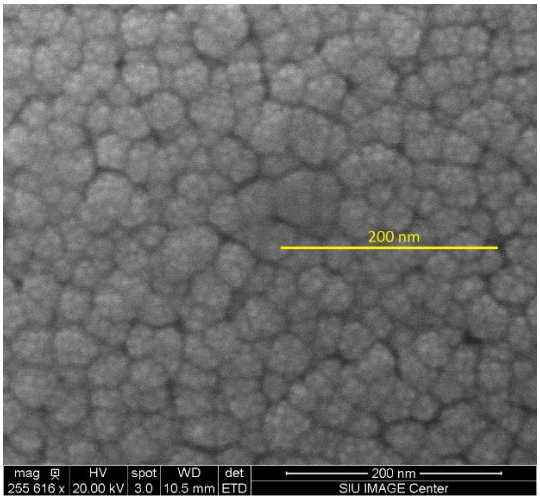

Fig. 22: Surface Image of CeO_2 (Magnification 255K X)

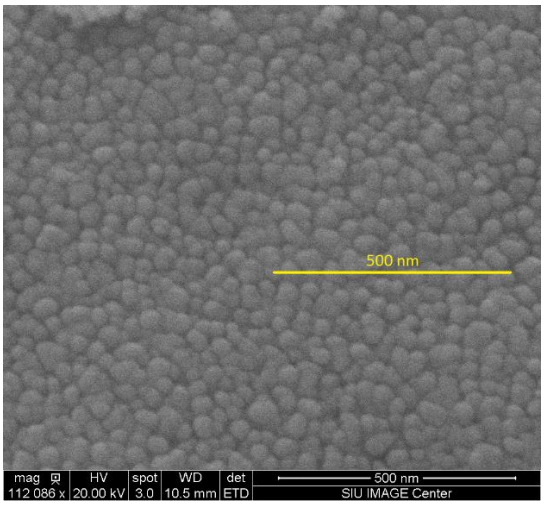

Fig. 23: Surface Image of $Ce_{0.95}Zr_{0.05}O_2$ (Magnification 112K X)

www.manaraa.com

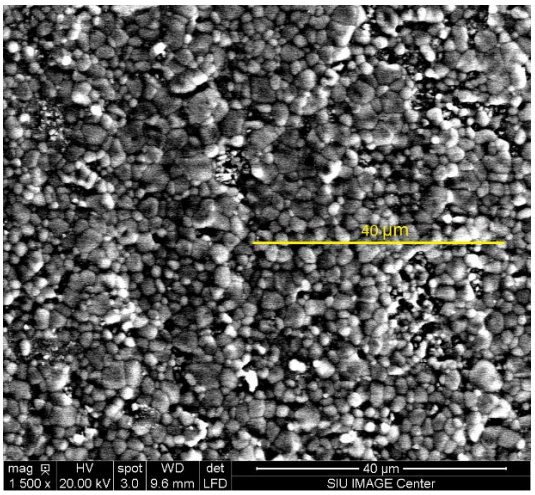

Fig. 24: Surface Image of $Ce_{0.9}Y_{0.05}Zr_{0.05}O_2$ (Magnification 1.5K X)

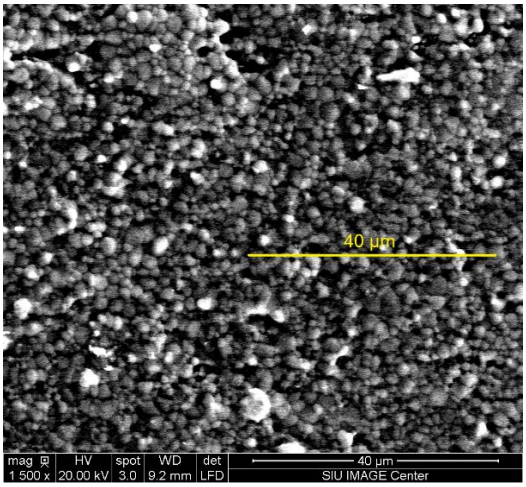

Fig. 25: Surface Image of $Ce_{0.9}Sc_{0.05}Zr_{0.05}O_2$ (Magnification 1.5K X)

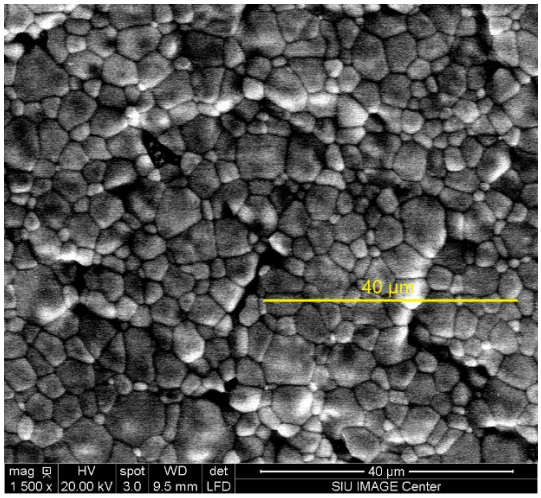

Fig. 26: Surface Image of $Ce_{0.9}Sm_{0.05}Zr_{0.05}O_2$ (Magnification 1.5K X)

www.manaraa.com

Figures 27 through 29 show the EDS mappings of $Ce_{0.9}Y_{0.05}Zr_{0.05}O_2$, $Ce_{0.9}Sc_{0.05}Zr_{0.05}O_2$, and $Ce_{0.9}Sm_{0.05}Zr_{0.05}O_2$. These mappings allow the distribution of the dopants to be known over the surface of these specimens.

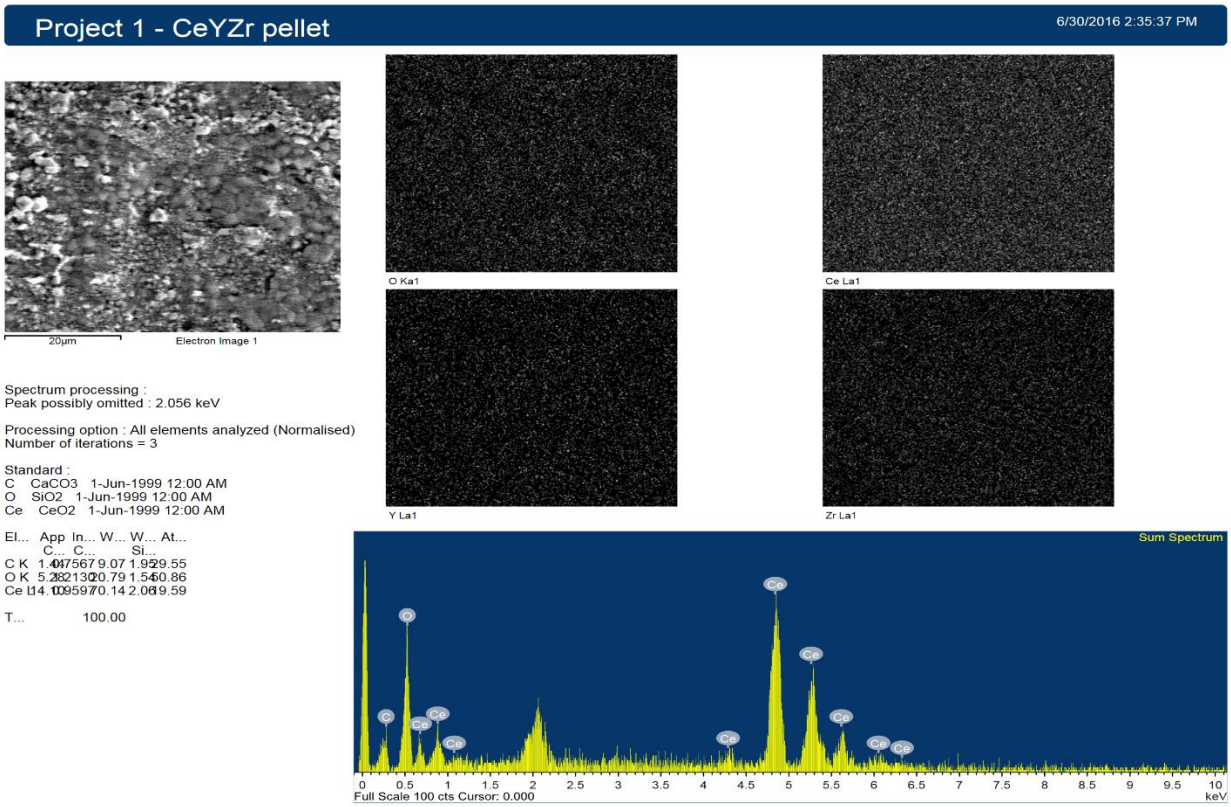

Fig. 27: EDS Mapping of $Ce_{0.9}Y_{0.05}Zr_{0.05}O_2$

www.manaraa.com

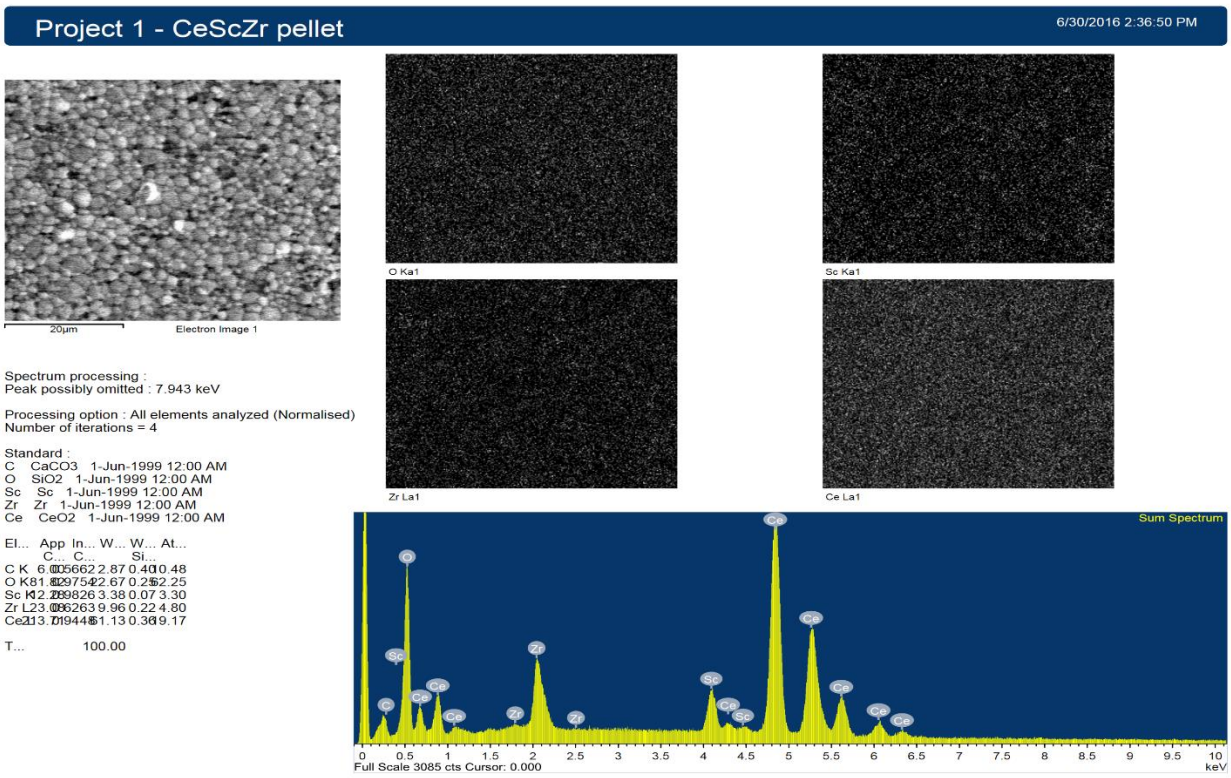

Fig. 28: EDS Mapping of $Ce_{0.9}Sc_{0.05}Zr_{0.05}O_2$

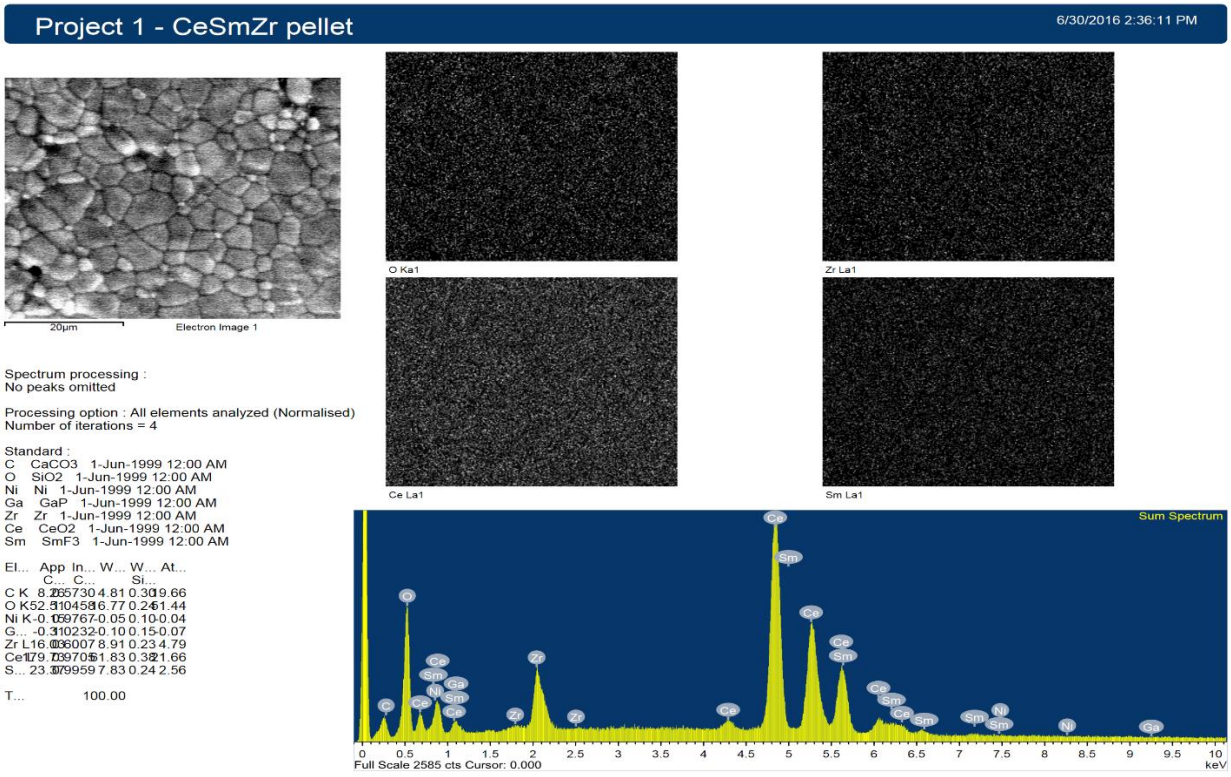

Fig. 29: EDS Mapping of $Ce_{0.9}Sm_{0.05}Zr_{0.05}O_2$

www.manaraa.com

CHAPTER 4

DISCUSSION

Table 1 shows the activation energy and σ_0 for all the samples. Activation energy is the amount of energy needed to be provided to increase the conductivity of the sample, while σ_0 is the theoretical conductivity of the sample at infinite temperature. From the table, it can be gathered that most of the samples have similar values for activation energy and σ_0. As there appears to be no direct relation between activation energy and σ_0, they should be compared individually to dopant valency and ionic radius.

Table 1: Activation Energy (E_a) and σ_0 for all Samples

Material	E_a (eV)	$\ln(\sigma_0)$ (mS·cm^{-1})
CeO_2	1.80E-03	24.4
$Ce_{0.95}Zr_{0.05}O_2$	3.88E-04	15
$Ce_{0.95}Y_{0.05}O_2$	9.74E-04	20.8
$Ce_{0.95}Fe_{0.05}O_2$	1.32E-03	21.2
$Ce_{0.95}Gd_{0.05}O_2$	9.48E-04	20.6
$Ce_{0.9}Y_{0.05}Zr_{0.05}O_2$	1.22E-03	20.8
$Ce_{0.9}Fe_{0.05}Zr_{0.05}O_2$	1.21E-03	22.3
$Ce_{0.9}Gd_{0.05}Zr_{0.05}O_2$	1.16E-03	19.9
$Ce_{0.9}Sc_{0.05}Zr_{0.05}O_2$	1.34E-03	21.1
$Ce_{0.9}Sm_{0.05}Zr_{0.05}O_2$	1.11E-03	20

www.manaraa.com

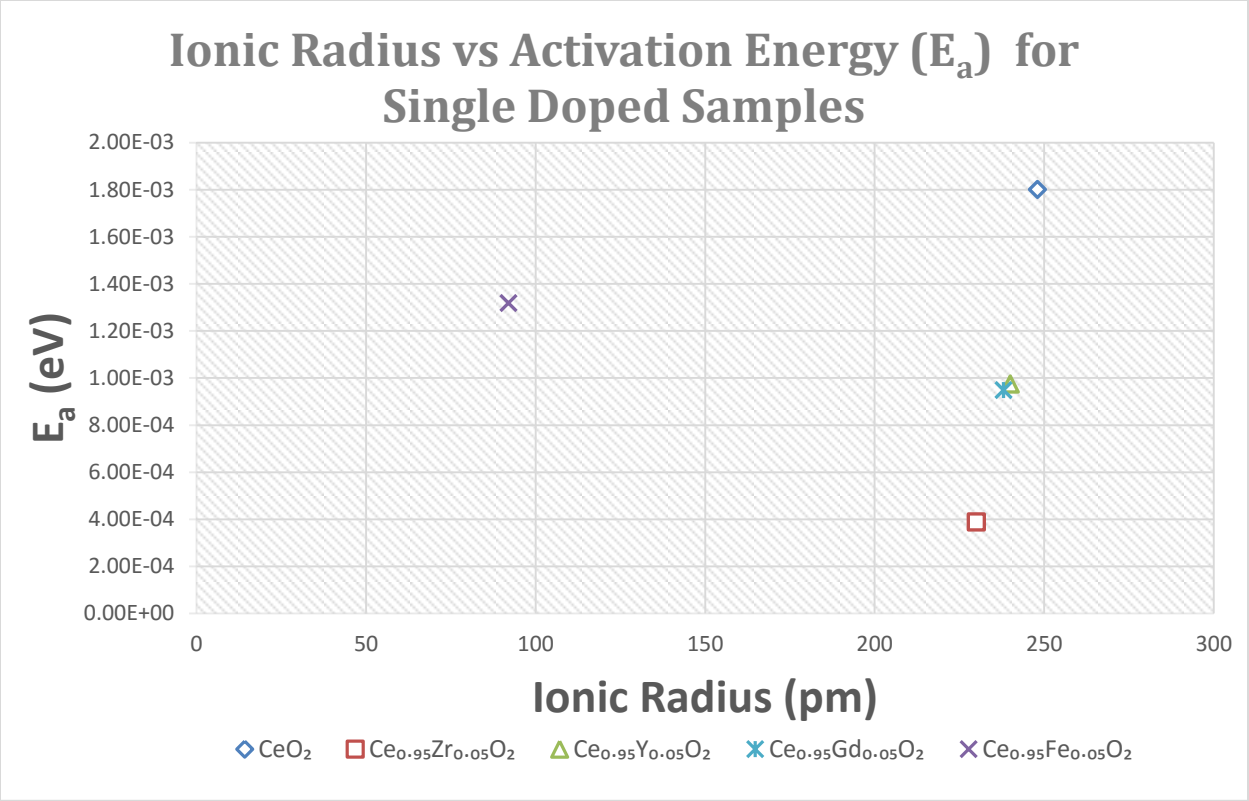

Fig. 30: Ionic Radius vs Activation Energy for Single Doped Samples

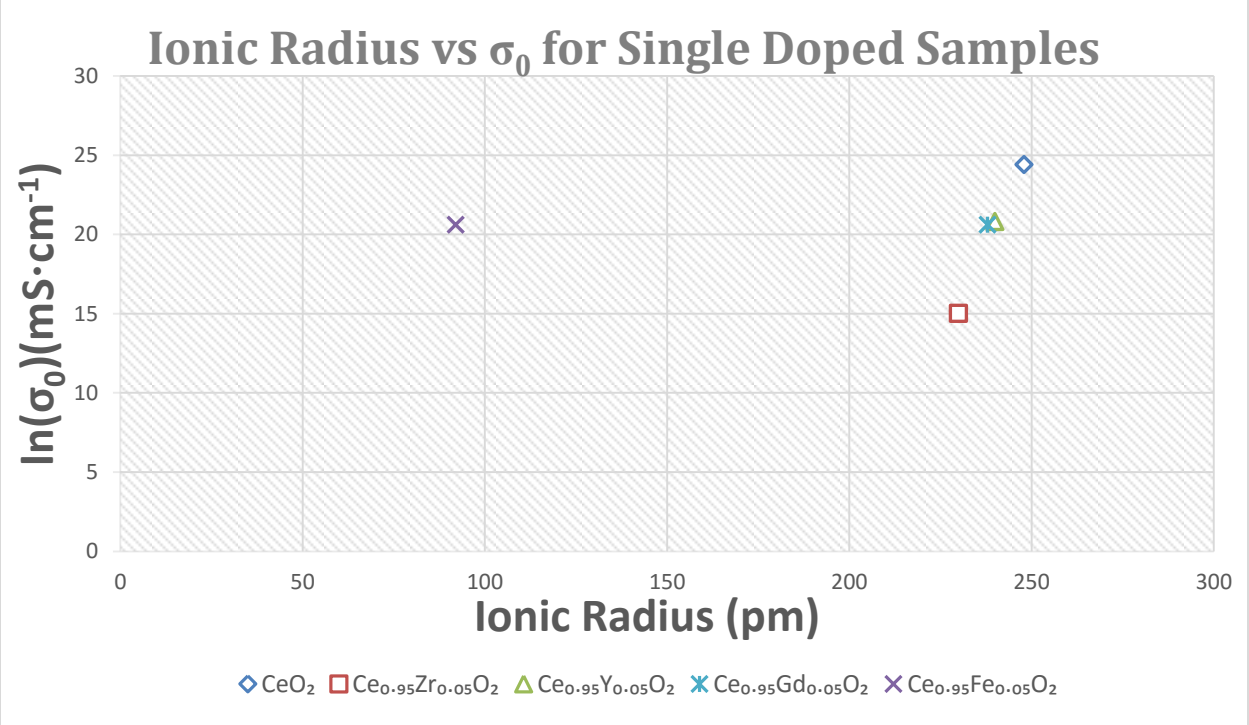

Fig. 31: Ionic Radius vs σ_0 for Single Doped Samples

www.manaraa.com

Figures 30 and 31 show the relationship between ionic radius and, both, activation energy and σ_0, respectively. With only one dopant being a divalent transition metal, it is hard to draw any concrete conclusion for comparing divalent dopants to trivalent or tetravalent dopants. However, one can see that the large difference in the ionic radius and valency of iron seems to cause it to behave much differently than the other dopants. When disregarding $Ce_{0.95}Fe_{0.05}O_2$, these graphs appear to show a positive linear relationship. With cerium having an ionic radius 248pm, this may indicate that oxygen holes become larger as the difference in the radius of the dopant to the radius of cerium grows. With these larger holes, it would require less energy to conduct the oxygen ions through the structure.

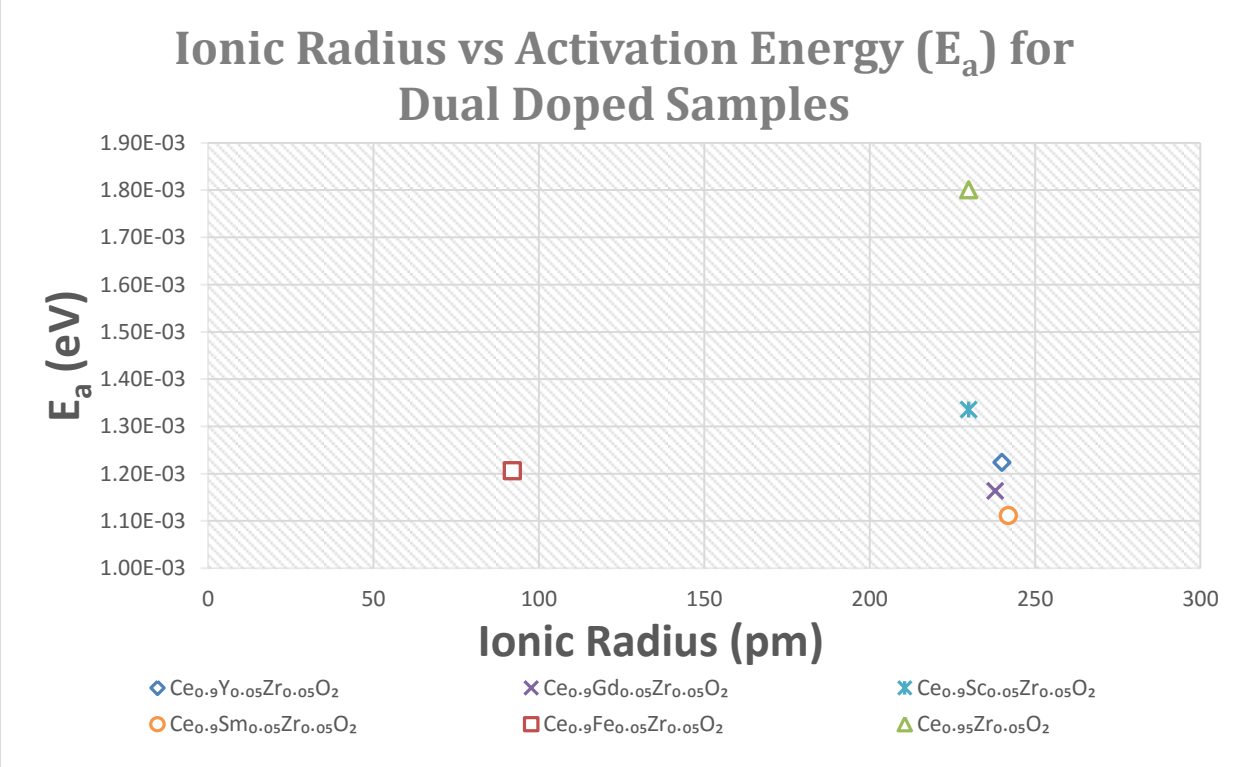

Fig. 32: Ionic Radius vs Activation Energy for Dual Doped Samples

www.manaraa.com

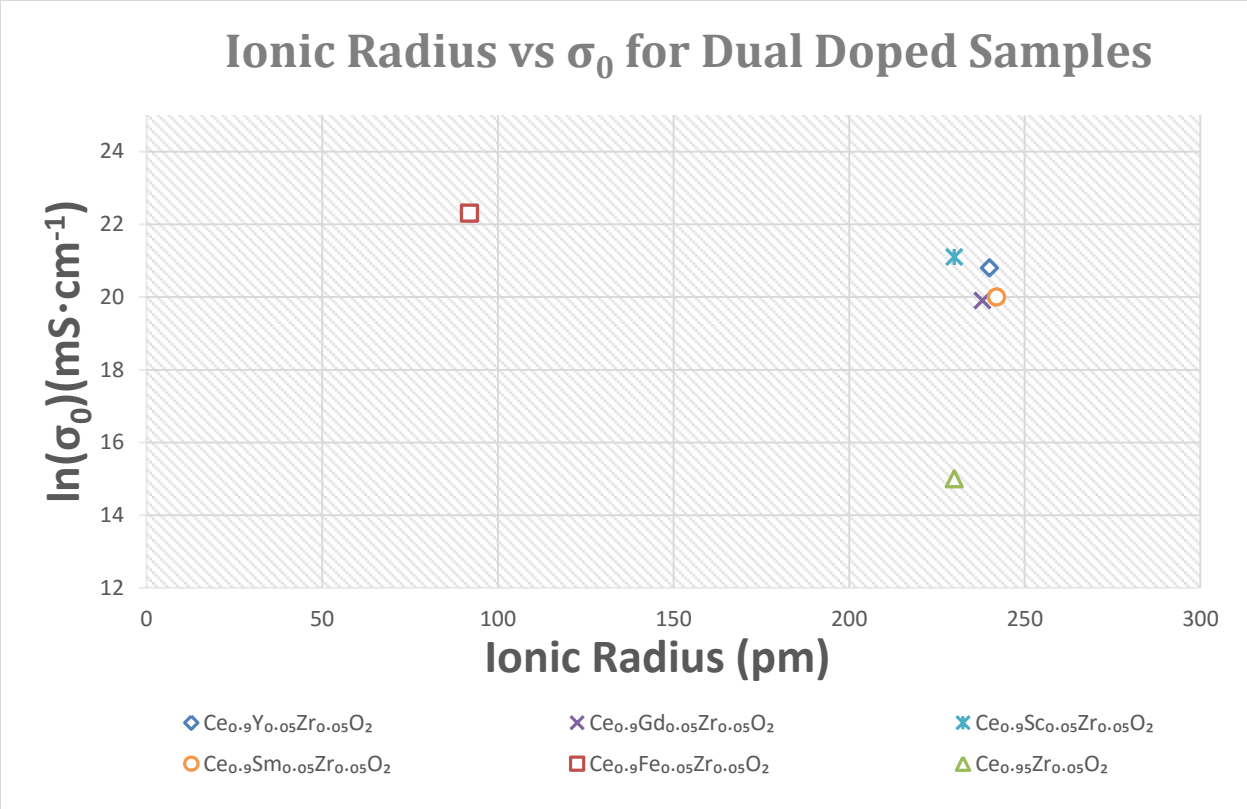

Fig. 33: Ionic Radius vs σ_0 for Dual Doped Samples

Figures, 32 and 33, show the same relationships to ionic radius as previously shown for the dual dopant samples. Figure 32 shows a slight negative linear relationship, when disregarding $Ce_{0.95}Fe_{0.05}O_2$. This appears to be due to the difference in the ionic radii between the two dopant and cerium. As the radii of the second dopant increases, the activation energy decreases. As for σ_0, there does not appear to be a clear relationship with ionic radius of the second dopant when doped with zirconium.

www.manaraa.com

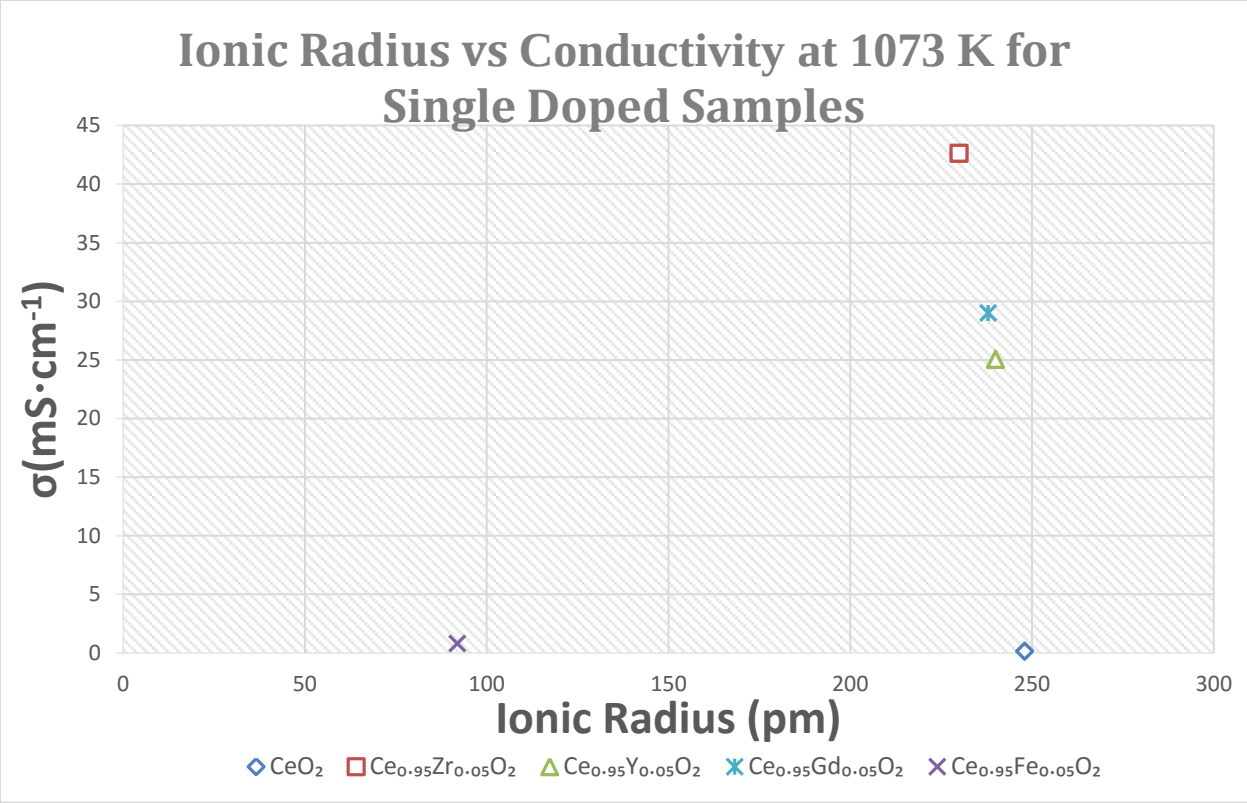

Fig. 34: Ionic Radius vs Conductivity at 1073 K for Single Doped Samples

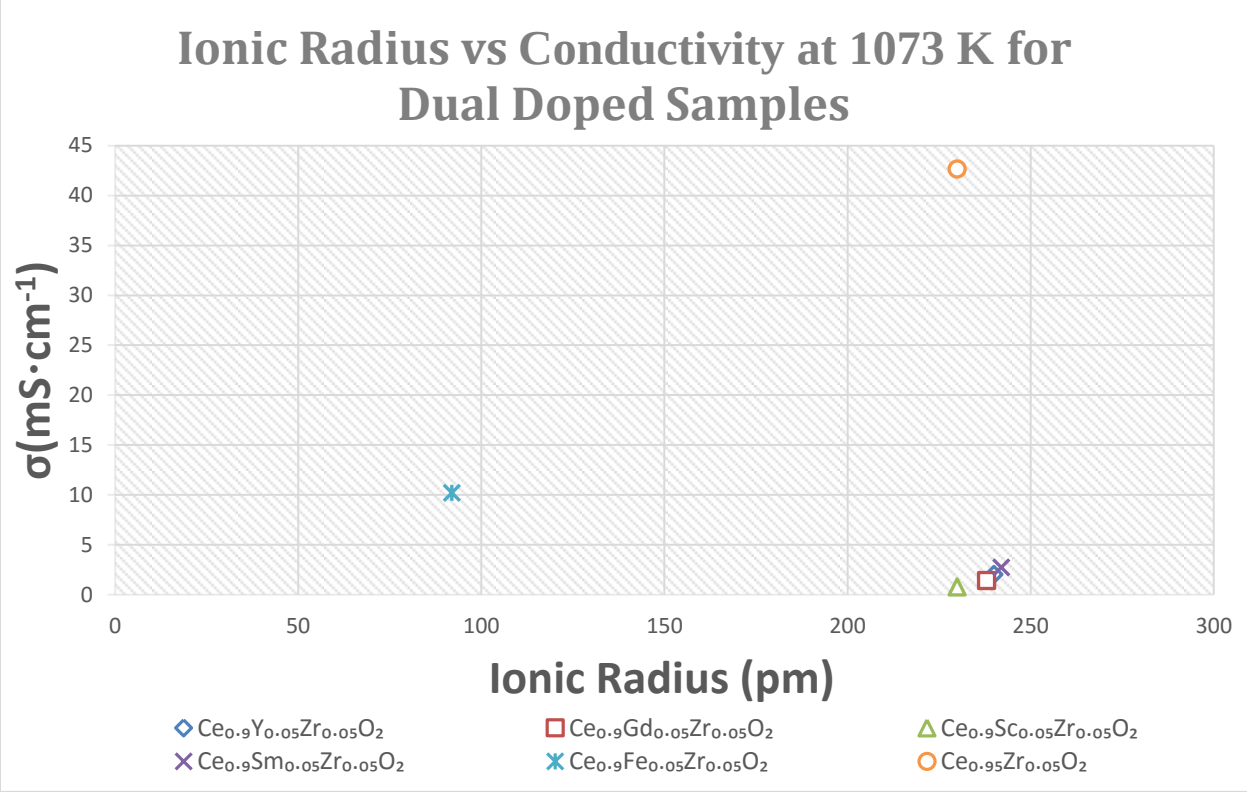

Fig. 35: Ionic Radius vs Conductivity at 1073 K for Dual Doped Samples

www.manaraa.com

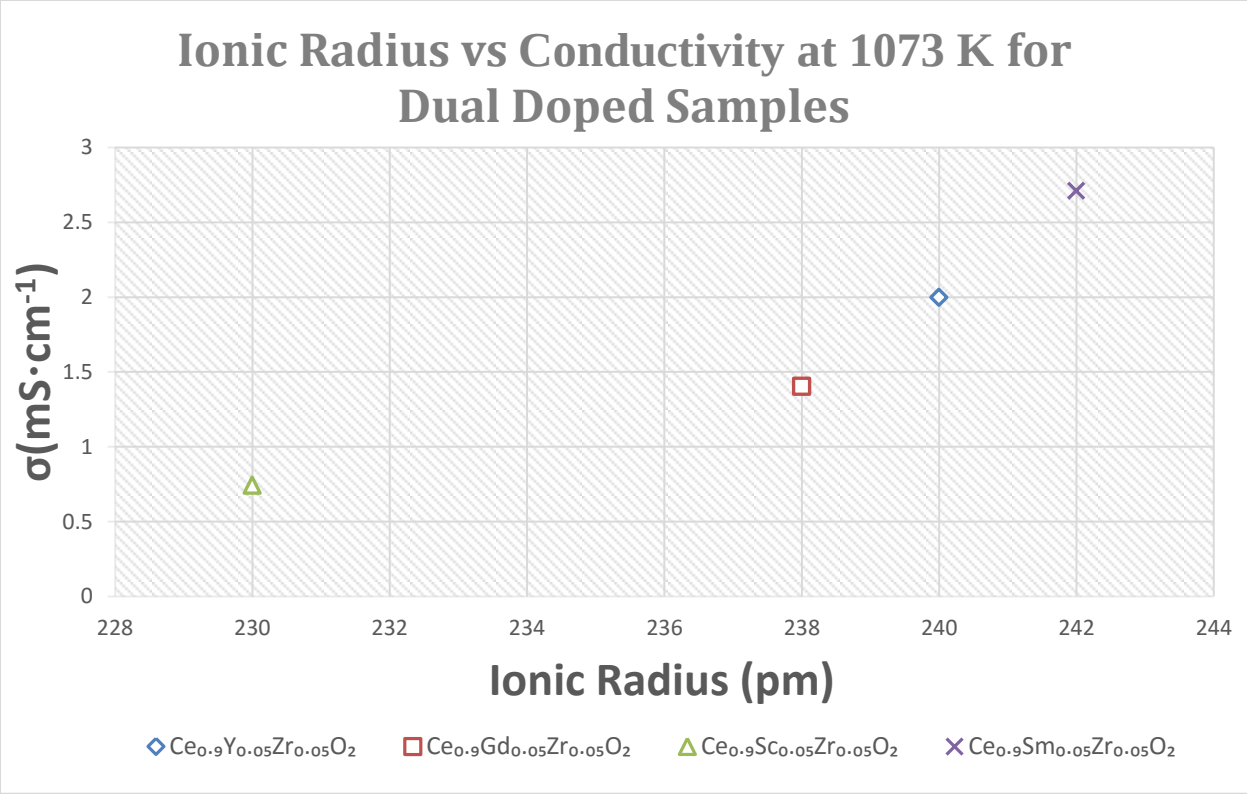

Fig. 36: Ionic Radius vs Conductivity at 1073 K for 3+ Ion Dual Doped Samples

Shown in figures 34 and 35 is the ionic radius vs conductivity at 1073K for single and dual doped samples, respectively. In figure 34, the addition of a trivalent or tetravalent dopant increase conductivity at the given temperature. However, the divalent dopant, iron, appears to have little to no effect on conductivity. The trivalent and tetravalent dopants also have a linear relationship with ionic radius, where a decrease in ionic radius increases conductivity. This relationship may be due to the increase in size of oxygen holes that are present in the structures. Figure 35 shows that the addition of a second dopant alongside zirconium has a negative impact on conductivity, with a slight positive linear relationship due to ionic radius for trivalent dopants. This impact may be due to the additional stress caused inside the microstructure, which could reduce the number and size of oxygen holes. Also note-worthy, the addition of iron as a second dopant, does not have as great of an effect.

www.manaraa.com

This is most likely due to both its size and valency not leading to the same loss in oxygen holes. Figure 36 shows the same relationship as figure 35, but with $Ce_{0.95}Fe_{0.05}O_2$ and $Ce_{0.95}Zr_{0.05}O_2$ removed. This shows that for dual doping with zirconium, an increase in ionic radius tends to increase the overall conductivity. Table 2 shows a summary of the conductivity results including the ionic radius and valency of the dopants.

Table 2: Summary of Conductivity Results

Material	E_a (eV)	$\ln(\sigma_0)$ ($mS \cdot cm^{-1}$)	Dopant R_{ionic} (nm)	Dopant Valency	σ @1073 K ($mS \cdot cm^{-1}$)
CeO_2	1.80×10^{-3}	24.4	248	NA	13.78×10^{-2}
$Ce_{0.95}Zr_{0.05}O_2$	3.88×10^{-4}	15.0	230	4+	42.62
$Ce_{0.95}Y_{0.05}O_2$	9.74×10^{-4}	20.8	240	3+	25.04
$Ce_{0.95}Fe_{0.05}O_2$	1.32×10^{-3}	21.2	92	2+	79.24×10^{-2}
$Ce_{0.95}Gd_{0.05}O_2$	9.48×10^{-4}	20.6	238	3+	28.99
$Ce_{0.9}Y_{0.05}Zr_{0.05}O_2$	1.22×10^{-3}	20.8	240, 230	3+, 4+	2.00
$Ce_{0.9}Fe_{0.05}Zr_{0.05}O_2$	1.21×10^{-3}	22.3	92, 230	2+, 4+	10.19
$Ce_{0.9}Gd_{0.05}Zr_{0.05}O_2$	1.16×10^{-3}	19.9	238, 230	3+, 4+	1.40
$Ce_{0.9}Sc_{0.05}Zr_{0.05}O_2$	1.34×10^{-3}	21.1	230, 230	3+, 4+	74.33×10^{-2}
$Ce_{0.9}Sm_{0.05}Zr_{0.05}O_2$	1.11×10^{-3}	20.0	242, 230	3+, 4+	2.71

Figure 37 is used to show that sintered density does not have a significant impact on conductivity when comparing different compounds. It shows that many compounds with similar densities have a wide range of conductivities. It is important to note that this figure does not compare the same compound with varying sintered density, as sintered density is expected to influence conductivity for the same compound.

www.manaraa.com

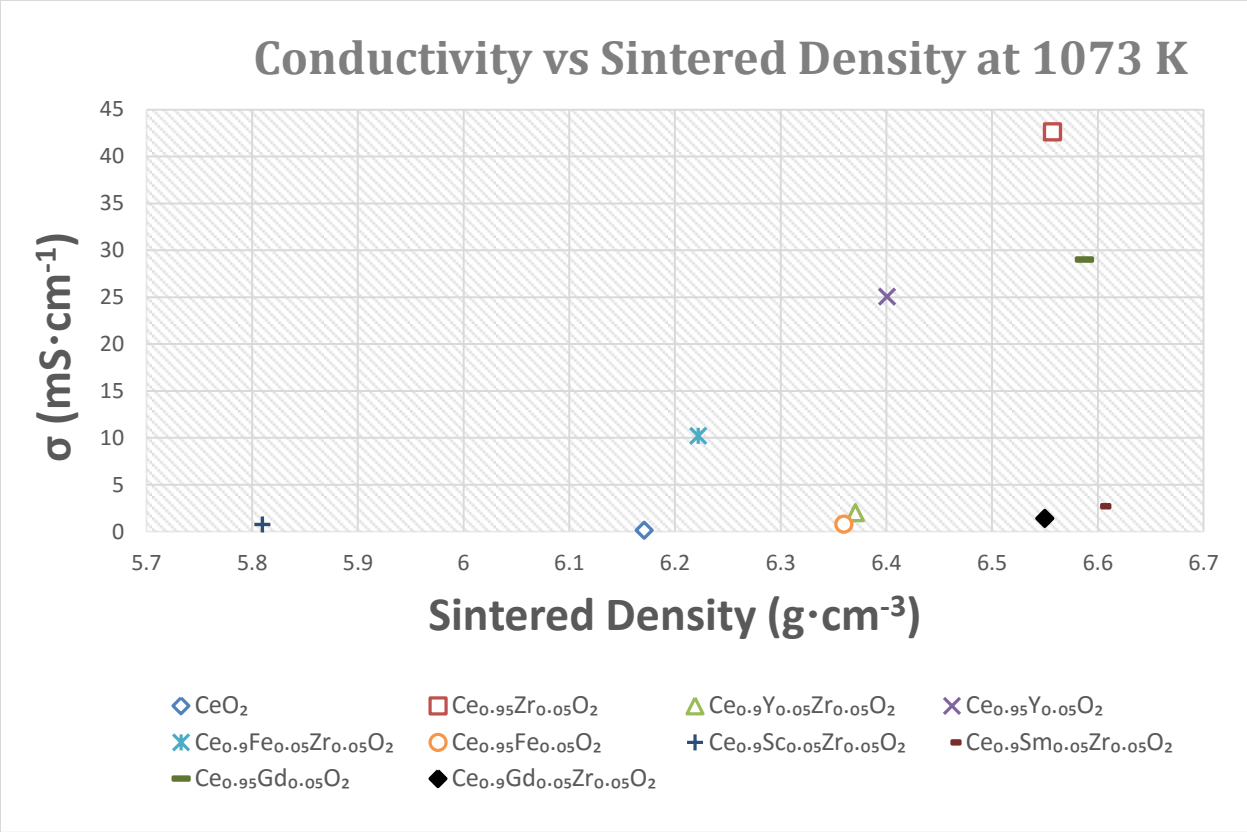

Fig. 37: Conductivity vs Sintered Density at 1073 K

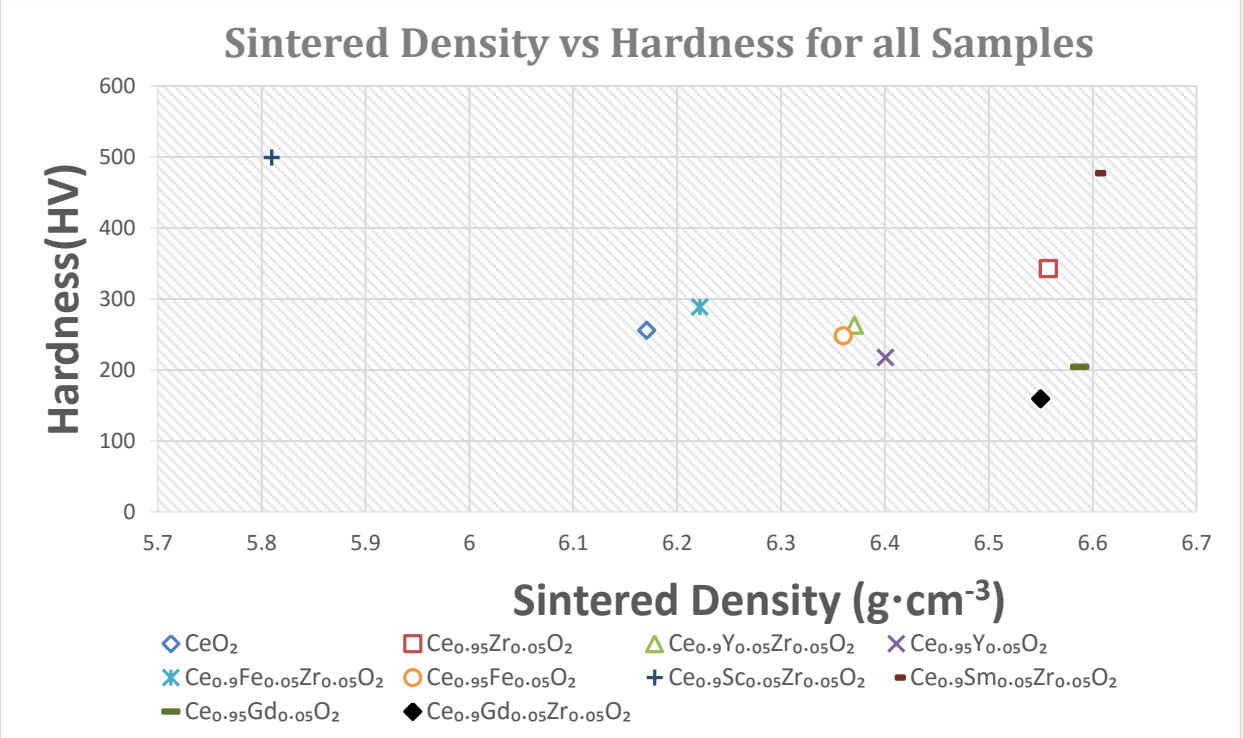

Fig. 38: Sintered Density vs Hardness for all Samples

www.manaraa.com

Figure 38 shows the relationship between sample sintered density and hardness. From the graph, there is no clear relationship between sintered density and hardness. Since there is no relationship, the difference in hardness could be attributed to the different dopants. It is possible that for the same dopant, sintered density could impact hardness.

The XRD, SEM, and EDS images all show expected results. Figures, 12 through 21, show XRD results for each sample. These graphs indicate that each sample, no matter the dopants, has the nearly the same structure as the undoped cerium oxide. Figures 22 through 26 show the surface images of each sample captured by SEM. Only figures 22 and 24 are of use as they use magnifications of 255K X and 112K X, respectively. The other images use a magnification of 1.5K X. With a large enough magnification grain size could be calculated. Figures 27 through 29 show EDS surface mappings of $Ce_{0.9}Y_{0.05}Zr_{0.05}O_2$, $Ce_{0.9}Sc_{0.05}Zr_{0.05}O_2$, and $Ce_{0.9}Sm_{0.05}Zr_{0.05}O_2$, respectively. From these images, it can be determined that each of the dopants in the respective samples are evenly dispersed. As each sample was prepared in the same fashion, it is assumed that the other samples have evenly distributed dopants as well.

From the above discussion and results, zirconium is the best dopant in terms of electrical conductivity. Due to the wide variety of studies for singular dopants, it is suggested to use samarium as the second dopant along with zirconium. This is due to the instability involved with using iron in the samples. Even though using iron as the second dopant appears to generate the highest electrical conductivity for the dual doped samples.

www.manaraa.com

CHAPTER 5

RECOMMENDATION FOR FUTURE WORK

It is recommended that samarium be used as the second dopant along with zirconium, unless other work is to be done. As such, suggestions for future work are given here. The conductivity that was studied in this research was overall conductivity tested in open air which includes electrical and ionic conductivities. As such, it is suggested that the conductivity is measured while supplying an oxygen deficiency to one side of the sample to get a better understanding of oxygen transfer rate. It is also suggested that the working temperature of any membrane used in a combustion system be known, this way an adequate material for said membrane can be chosen. As for other studies on these same materials, a dopant quantitative analysis should be performed as well. Meaning variations in the amount of a specific dopant should be compared.

www.manaraa.com

REFERENCES

[1] Sunarso, J., Baumann, S., Serra, J.M., Meulenberg, W.A., Liu, S., Lin, Y.S., Diniz Da Costa, J.C., 2008, “Mixed Ionic-Electronic Conducting Ceramic-Based Membranes for Oxygen Separation”, Journal of Membrane Science, 320, pp. 13-41.

[2] Andersson, David A., Simak, Sergei I., Skorodumova, Natalia V., Abrikosov, Igor A., Johansson, Börje, 2005, “Optimization of Ionic Conductivity in Doped Ceria,” PNAS, 103 (10), 3518-3521

[3] Kharton, V. V., Figueiredo, F. M., Navarro, L., Naumovich, E. N., Kovalevsky, A. V., Yaremchenko, A. A., Viskup, A. P., Carneiro, A., Marques F. M. B., Frade, J. R., 2001, “Ceria-based Materials for Solid Oxide Fuel Cells,” Journal of Materials Science, 36, pp. 1105-1117.

[4] Higashi, Kenji, Sonoda, Kazutoshi, Ono, Hiroshi, Sameshima, Soichiro, Hirata Yoshihiro, 1999, “Synthesis and Sintering of Rare-Earth-Doped Ceria powder by the Oxalate Coprecipitation Method,” Journal of Materials Research, 14 (3), 957-967

[5] Inaba, Hideaki, Tagawa, Hiroaki, 1996, “Ceria-based Solid Electrolytes,” Solid State Ionics, 83, pp. 1-16.

[6] Gerhardt-Anderson, R., Nowich, A. S., 1981, “Ionic Conductivity of CeO_2 with Trivalent Dopants of Different Ionic Radii,” Solid State Ionics, 5, pp. 547-550.

[7] Nagabhushana, Nagendra, Lane, Jonathan Andrew, Christie, Gervase Maxwell, van Hassel, Bart Antonie, 2009, “Composite Oxygen Ion Transport Membrane,” U.S. Patent 7556676.

www.manaraa.com

[8] Rayford, II, Cleveland E., 2008, “Characterization of WC and TiC Based Cermets for Solid Oxide Fuel Cell Interconnect Application,” M.S. thesis, Mechanical Engineering, Southern Illinois University Carbondale

[9] Kong, Jia Huey, 2016, “Sintering Properties of TiC-Ni-Mo Cermet Using Nanosized TiC Powders,” M.S. thesis, Mechanical Engineering, Southern Illinois University Carbondale

www.manaraa.com

VITA

Graduate School
Southern Illinois University

James C. Morrow

jcmorrow89@gmail.com

Southern Illinois University Carbondale
Bachelor of Science, Mechanical Engineering, May 2011

Thesis Title:
Investigation of the Material Properties of Cerium Oxide with Dopants for an Oxygen Transport Membrane

Major Professor: Dr. Kanchan Mondal

www.manaraa.com